Quaternary Geochronology 89 (2025) 101686

Contents lists available at ScienceDirect

Quaternary Geochronology

journal homepage: www.elsevier.com/locate/quageo

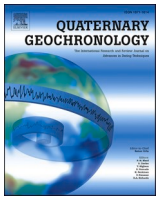

Developing robust lake sediment chronologies using ^{210}Pb, Pu and radiocarbon dating of pollen concentrates and macrofossil: A case study from Lake Surprise, Victoria, Australia

Asika Dharmarathna [a,*], Haidee Cadd [b], Cameron Barr [a,c], Alexander Francke [a,c], Quan Hua [d], David Child [d], Michael Hotchkis [d], Atun Zawadzki [d], Patricia Gadd [d], Chris Turney [b], Christopher E. Marjo [b], John Tibby [c,e], Jonathan J. Tyler [a,c]

[a] School of Chemistry, Physics and Earth Sciences, The University of Adelaide, South Australia, Australia
[b] Chronos ^{14}Carbon-Cycle Facility, Mark Wainwright Analytical Centre, University of New South Wales, Sydney, Australia
[c] Sprigg Geobiology Centre, The University of Adelaide, Adelaide, South Australia, Australia
[d] Australian Nuclear Science and Technology Organisation (ANSTO), Sydney, New South Wales, Australia
[e] Department of Geography, Environment and Population, The University of Adelaide, Adelaide, South Australia, Australia

ARTICLE INFO

Keywords:
Pollen radiocarbon dating
^{210}Pb dating
Pu isotopes
Fourier transform infrared (FTIR)
Bayesian plum modelling
Lake sediment

ABSTRACT

The development of reliable sediment chronologies is crucial for accurate interpretations of decadal to century-scale palaeoenvironmental changes in the late Quaternary. Although radiocarbon dating of sedimentary sequences is commonly undertaken, not all the organic fractions are representative of atmospheric ^{14}C levels, resulting in inaccurate age models. Whilst terrestrial plant macrofossils are widely considered ideal dating material – assuming they are contemporaneous with the horizons being dated – they are often sparse or absent. In this context, radiocarbon dating of pollen extracts is increasingly being used as alternative dating material. Here, we used pollen radiocarbon dating, alongside a suite of macrofossil and bulk sediment dates, to develop a chronology for the Holocene sediments of Lake Surprise, in Victoria, Australia. ^{210}Pb activity and Plutonium (Pu) concentrations and isotope ratios were also analysed to constrain the age of the uppermost sediments, augmented with recent historical markers, including the first arrival of *Pinus* pollen and the date of an earlier coring expedition at the site in 2004. With respect to the radiocarbon dates, we found an age offset between the plant macrofossils and bulk sediment dates of 260 ± 86 ^{14}C years and an offset of ~340 ^{14}C years between plant macrofossil and pollen extracts. In both cases, macrofossil dates appeared to be "younger" than the bulk sediment and pollen dates. The offset between pollen and plant macrofossil dates was found to vary with sediment depth and generally correlate with carbonate concentration in the sediment. Using Fourier transform infrared spectroscopy (FTIR), we determined that the pollen extracts were not contaminated by either carbonate or charcoal. However, contamination by algal spores could not be ruled out, and we hypothesise that those algal spores may have assimilated aged dissolved inorganic carbon during periods of higher groundwater influx, thus altering the measured radiocarbon age of the pollen extract. Macrofossil and corrected pollen radiocarbon dates were incorporated in a Bayesian age-depth model which integrated ^{210}Pb activities and Pu data and bomb pulse C-14 dates validated using recent historical age markers. Our results suggest that it is possible to generate a robust geochronological framework for Lake Surprise using radiocarbon dating back to at least ~10,846 cal yr BP.

1. Introduction

1.1. The need for lake sediment chronologies in south-eastern Australia

Lake sediments are important archives of climate and environmental changes, extending the instrumental (observational) record and providing a long-term context for human impacts, ecological change, and climate over tens to thousands of years. However, reconstructions of environmental and climate change require an accurate and reliable chronological framework to assess the timing and duration of events

* Corresponding author. School of Chemistry, Physics and Earth Sciences, The University of Adelaide, South Australia, Australia.
E-mail addresses: asika.dharmarathna@adelaide.edu.au, ashi.uop@gmail.com (A. Dharmarathna).

https://doi.org/10.1016/j.quageo.2025.101686
Received 6 May 2024; Received in revised form 3 June 2025; Accepted 6 June 2025
Available online 11 June 2025

being inferred (Howarth et al., 2013; Corcho-Alvarado et al., 2014; Zimmerman and Wahl, 2020; Tunno et al., 2021; Rivera-Araya et al., 2022). Among numerous dating techniques employed so far, the most widely used methods for Holocene lacustrine sediments are radiocarbon (^{14}C) dating of terrestrial macrofossils and ^{210}Pb dating of recent sediments, however, neither method is without challenges (Appleby, 2001; Björck and Wohlfarth, 2001; Wolfe et al., 2004; Brenner and Kenney, 2015; Strunk et al., 2020). Lake sediment records are particularly important for south-eastern Australia, where environmental challenges such as prolonged droughts, catastrophic wildfires and widespread loss of biodiversity highlight the need for long-term context to guide management actions (Barr et al., 2014; Kiem et al., 2016; Tibby et al., 2018; Mariani et al., 2022). Nevertheless, most of the available sediment records heavily depend on limited chronologies, which sets a major drawback for accurate interpretations from these studies (Fletcher and Thomas, 2010; Gouramanis et al., 2013; Woodward et al., 2014; De Deckker, 2022). As a result, there is an increasing demand for robust chronologies from the region.

This study attempts to develop an age model for the Holocene sediments of Lake Surprise, which is an important palaeoclimate archive for south-eastern Australia and is situated in the World-Heritage listed Budj Bim Cultural Landscape (Timms, 1976; Builth et al., 2008; Barr et al., 2014; Falster et al., 2018; Dharmarathna, 2022). Previous chronologies for the Holocene and late Pleistocene sediments of Lake Surprise have used a combination of bulk sediment and pollen radiocarbon dates, as well as ^{210}Pb analyses (Builth et al., 2008; Barr et al., 2014; Falster et al., 2018). These studies encountered a range of issues during the development of chronologies related to contamination and possible groundwater effects. Furthermore, to date, there is no continuous high-resolution chronology that links the Holocene sediments (Builth et al., 2008; Falster et al., 2018), through the Common Era (Barr et al., 2014) to the present day. We aimed to address these limitations in this study by using a modified pollen extraction procedure (Cadd et al., 2022) and by screening pollen extracts for contamination using FTIR spectroscopy. Furthermore, ^{210}Pb, Pu analyses and post-bomb ^{14}C analyses were combined using the Bayesian *Plum* model to develop a continuous age model of the sediment sequence with quantified age uncertainty (Aquino-López et al., 2018).

1.2. ^{210}Pb dating of recent lake sediments

Atmospheric fallout of ^{210}Pb in lake sediments is used widely to obtain recent (100–200 years) chronological information in lake sediments due to the relatively short half-life of ^{210}Pb (~22.3 years) (Appleby and Oldfield, 1978; Appleby et al., 1979; Appleby, 2008; Aquino-López et al., 2018, 2020a). ^{210}Pb binds to atmospheric aerosols and is incorporated in lacustrine sediments (Appleby, 1998, 2001; Heijnis, 2001). Unsupported or "excess" ^{210}Pb from atmospheric influx contributes the majority of Pb in lake sediments, whereas "supported" ^{210}Pb from in-situ decay of ^{226}Ra from the catchment contributes a lesser amount (Appleby, 2001). In recent decades, three models have been used to define the ^{210}Pb chronologies of lake sediments: the Constant Rate of Supply (CRS) model for lakes with non-uniform sediment accumulation rates, and the Constant Flux Constant Sedimentation (CFCS) and Constant Initial Concentration (CIC) models, which are applicable when a constant accumulation rate can be assumed (Goldberg, 1963; Krishnaswamy et al., 1971; Appleby and Oldfield, 1978; Appleby et al., 1979; Appleby, 2001; Kirchner, 2011; Sanchez-Cabeza and Ruiz-Fernández, 2012; Aquino-López et al., 2020a). More recently, a Bayesian approach to modelling ^{210}Pb has emerged as *"Plum"*, which requires fewer assumptions about atmospheric fallout rates or sediment accumulation (Aquino-López et al., 2018). Instead, the model uses prior information on ^{210}Pb, radiocarbon and other dates (e.g. OSL, Tephra etc). In the *Plum* modelling, the dated depths in a core are segmented into thin vertical sections. Through extensive Markov Chain Monte Carlo (MCMC) iterations, Plum calculates the ^{210}Pb flux, supported ^{210}Pb, and the accumulation rate (in years/cm) for each of these segments (Aquino-López et al., 2020a).

Given that lake and catchment environments are complex and may cause deviations from the ideal monotonic decline of unsupported ^{210}Pb in the sediment, ^{210}Pb chronologies should be validated using other markers (Appleby, 2001, 2008; Smith, 2001; Holmgren et al., 2010; Kirchner, 2011; Barsanti et al., 2020). During the 20th century, nuclear bomb testing led to the widespread release and dispersal of several artificial radionuclides (^{137}Cs, ^{239}Pu, ^{240}Pu, ^{241}Am), which subsequently accumulated in sedimentary environments (UNSCEAR, 2000; Leslie and Hancock, 2008; Hancock et al., 2011; Corcho-Alvarado et al., 2014; Harrison et al., 2021). Recent research has emphasised mass spectrometric measurement of Pu isotopes (^{239}Pu and ^{240}Pu) which can be measured at relatively low concentrations with long half-lives ($2.4*10^4$ and $6.5*10^3$ years for ^{239}Pu and ^{240}Pu respectively), which make up the majority of the Pu activity linked to nuclear weapon fallout (Leslie and Hancock, 2008; Hancock et al., 2011; Harrison et al., 2021).

The ^{240}Pu/^{239}Pu isotope ratio provides valuable insights into the sources and transport of Pu fallout in the environment (Kelley et al., 1999; Jakopi et al., 2010; Zheng et al., 2012; Harrison et al., 2021). When combined with other Pu isotope ratios (^{241}Pu/^{239}Pu), it provides detailed information about the origin of Pu sources (Jakopi et al., 2010). However, published data on these minor isotope ratios are limited, and only a few studies reported combined isotope ratios for the same sample (Kelley et al., 1999; Jakopi et al., 2010; Zheng et al., 2012). Scatter plots of ^{240}Pu/^{239}Pu vs ^{241}Pu/^{239}Pu atom ratios are used to distinguish between global and local/regional fallout. The ^{240}Pu/^{239}Pu ratio of global fallout from atmospheric nuclear weapons testing exhibits a characteristic mean value of 0.185 ± 0.047 in the Southern Hemisphere, while the corresponding ^{241}Pu/^{239}Pu ratio is typically around 0.00197 ± 0.00093 (Kelley et al., 1999). In contrast, local/regional fallout, such as that of Pu isotopes originating from nearby test sites, can display markedly different isotope ratios. Previous studies have shown that the ^{240}Pu/^{239}Pu ratios of environmental samples originated from Australian nuclear test sites are significantly lower than the global fallout average (Everett et al., 2008; Child and Hotchkis, 2013; Tims et al., 2013, 2016; Johansen et al., 2016, 2019; Smith et al., 2016; Harrison et al., 2021).

Previous studies have highlighted the limitations of CFCS and CRS modelling even with the introduction of chronological markers due to the reliance on assumptions about sediment accumulation rates and the need to interpolate ages (Kirchner, 2011; Baskaran et al., 2014; Tylmann et al., 2016; Aquino-López et al., 2018; Abril, 2019). The most common drawbacks are inconsistencies in ages derived from different model calculations, inaccurate sediment accumulation rates and significant uncertainties in model assumptions (Tylmann et al., 2016; Aquino-López et al., 2018). It is also possible that in some cases external or post-depositional processes such as erosion, sediment transport, and mixing cannot be considered in developing ^{210}Pb chronologies (e.g. Barsanti et al., 2020). When the ^{210}Pb profile does not reach equilibrium, missing ^{210}Pb data is estimated through interpolation or extrapolation of sediment core data, further challenging the development of reliable age estimates (Appleby, 2001; Aquino-López et al., 2020a).

To address many of these limitations, Aquino-López et al. (2018) introduced the Bayesian *Plum* model as an alternative way of determining sediment age from ^{210}Pb data. This model utilises Bayesian approaches to estimate chronological uncertainty and incorporates the behaviour of unsupported and supported ^{210}Pb. *Plum* is an extension of the well-established age-depth function *Bacon*, which enables the inclusion of radiocarbon dates into the chronology (Blaauw and Christen, 2011; Aquino-López et al., 2018; Blaauw et al., 2020). The *Plum* approach, tested and compared to the most widely used CRS model elsewhere, has been proven to be reproducible, accurate in measuring uncertainties, and effective in cases where the ^{210}Pb profile is incomplete (Aquino-López et al., 2020a, 2020b).

1.3. Radiocarbon dating of lake sediments

Radiocarbon (^{14}C) dating is largely used to determine the age of various carbon-bearing materials over the past ~50,000 years, relying on the radioactive decay of ^{14}C. It has also been used to trace "bomb-pulse" ^{14}C from atmospheric nuclear weapon testing during the 1950s–1980s and has been applied as a potent dating tool, providing dating accuracies ranging from one to a few years in contemporary terrestrial materials (Hua et al., 2012, 2013, 2022). However, ^{14}C analysis of bulk sediment can generate age-estimation errors due to sediment heterogeneity and contributions by "old" carbon, derived from geologic sources, or "young" carbon, which has either migrated through the sediment (e.g. humic acids) or which is synthesised *in situ* by bacterial activity (Björck and Wohlfarth, 2001; Kilian et al., 2002; Howarth et al., 2013; Strunk et al., 2020; Cadd et al., 2022).

Terrestrial macrofossils (e.g. leaves, seeds, needles and twigs) found in lake sediments are crucial for accurate radiocarbon dating due to their equilibrium with atmospheric $^{14}CO_2$ and resistance to migration through the sediment profile (Olsson, 1983; Marty and Myrbo, 2014; Meng et al., 2020; Norris et al., 2020). Further, their rapid degradation leads to short residence times in lake catchments before deposition (Howarth et al., 2013; Norris et al., 2020). However, macrofossils are not always abundant enough in depositional environments, particularly in semi-arid and high-altitude regions (Kilian et al., 2002; Fletcher et al., 2017; Cadd et al., 2022). In such cases, pollen grains that are ubiquitous and of terrestrial origin are considered a suitable substitute for ^{14}C dating (Howarth et al., 2013; Fletcher et al., 2017; Tunno et al., 2021; Cadd et al., 2022). Pollen grains are well-preserved in reducing lake sediments due to their chemical resistance and are found in a variety of sedimentary settings (Björck et al., 2001; Fletcher et al., 2017).

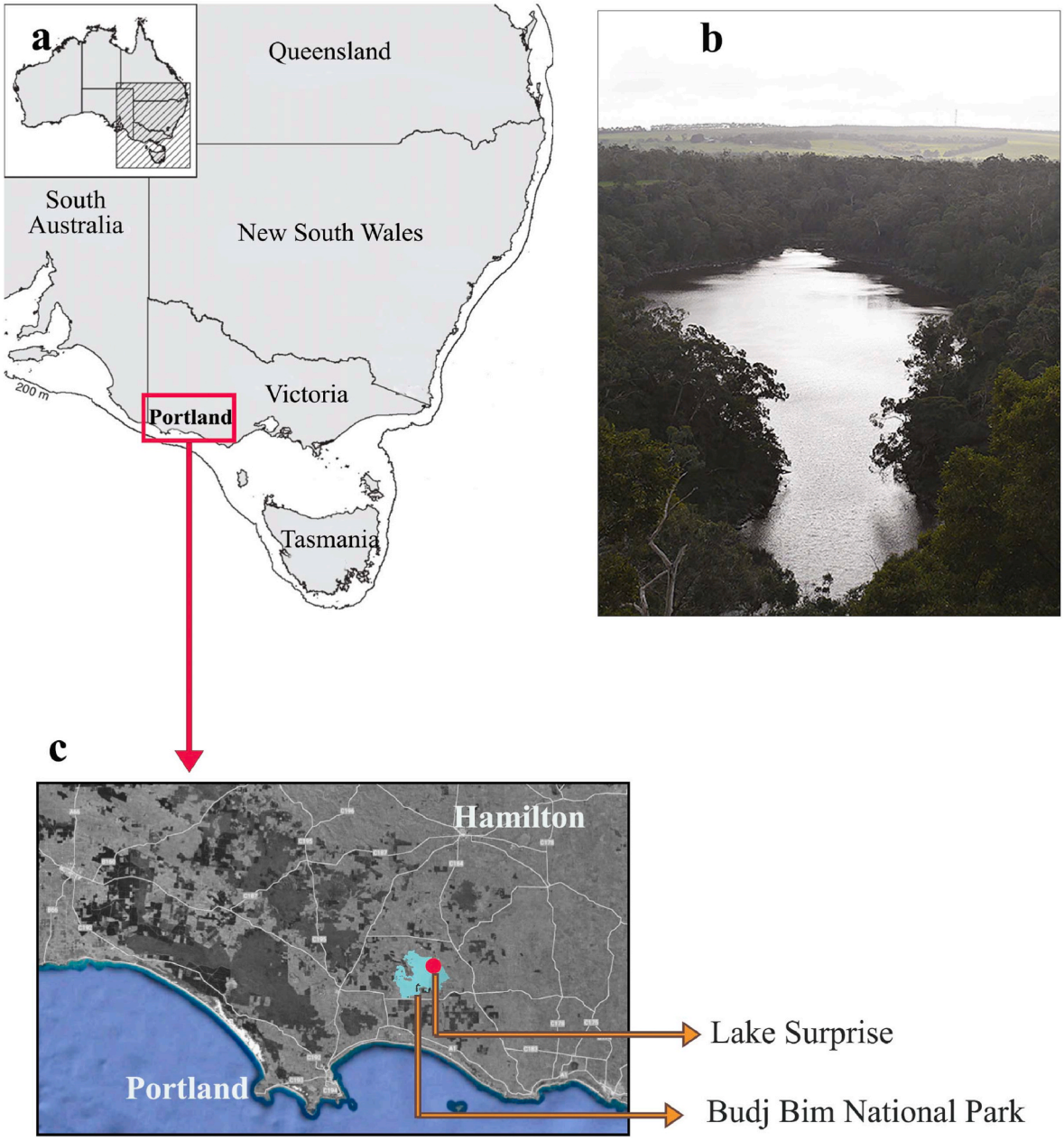

Fig. 1. a) Map of south-east Australia representing the approximate location of western Victoria (Graham and Daley, 2011), b) Lake Surprise looking north-west from the crater rim of Mt Eccles (Falster et al., 2018) c) Zoomed-in section of the selected region of western Victoria representing the location of Lake Surprise and the Budj Bim National Park (source: Google Earth version 10.45.0.3).

However, the use of pollen grains as the primary source of dating of lacustrine sediments remains uncommon, due to the complex nature of pollen extraction procedures (Fletcher et al., 2017; Cadd et al., 2022). Challenges include the possibility of reworked or anachronous pollen grains, prolonged processing times, and incomplete removal of non-pollen material from the resulting pollen concentrate (Tennant et al., 2013; Martin et al., 2019; Cadd et al., 2022). As a consequence, several studies have attempted to improve these methods over the last few decades (Long et al., 1992; Mensing and Southon, 1999; Tennant et al., 2013; Martin et al., 2019; Tunno et al., 2021; Cadd et al., 2022).

2. Materials and methods

2.1. Study site

Lake Surprise, a crater lake formed around 37,000 years ago (Matchan et al., 2020), is located in the Budj Bim National Park in the volcanic plains of western Victoria (Fig. 1c), whereby volcanic basalts, scoria cones and maars intersect a basement of Cretaceous sandstone, Tertiary-Quaternary marl and limestone (Price et al., 1997; Barr et al., 2014). The lake experiences a temperate climate of hot dry summers and mild wet winters with the majority of the rainfall occurring in the winter (Australian Bureau of Meteorology, 2021). The amalgamation of three adjacent volcanoes formed the ~11.5 m deep lake, which is ~600 m long, 200 m wide and which has an irregularly shaped lake surface with larger littoral habitats at each end (Fig. 1b) (Timms, 1976; Dharmarathna, 2022). Lake Surprise has been considered a "closed basin" due to the absence of any fluvial input or output to or from the lake (Barr et al., 2014). However, while the lake is fed predominantly by precipitation, groundwater inflow and outflows can be inferred based on lake water geochemistry (Dharmarathna, 2022), and these groundwater influences are anticipated to have a particular impact during dry spells (Falster et al., 2018). Densely vegetated, steep and high (~49 m) crater walls function as wind barriers that prevent deep mixing and retain distinct boundaries during lake stratification (Timms, 1976; Builth et al., 2008; Barr et al., 2014; Falster et al., 2018). The small and steep catchment is heavily vegetated by *Eucalyptus viminalis* ("manna gum") and *Acacia melanoxylon* ("blackwood") (Builth et al., 2008; Barr et al., 2014). The understorey is comprised of *Pteridium esculuntum* ("bracken"), *Banksia marginanta*, Poaceae and Asteraceae species (Tibby et al., 2006). Shallow water margins are home to a diverse, though typically restricted zone of aquatic vegetation made up primarily of emergent macrophytes and floating plants in protected open water (Tibby et al., 2006; Falster et al., 2018).

2.2. Coring and core sampling

Three series of sediment cores were recovered from the lake in 2019. Two 10 m long overlapping sediment cores (SUR-19-02 & SUR-19-03) were collected as 1 m segments using a modified large-bore Bolivia piston corer with an internal diameter of 63 mm (Appendix, Fig. A2) (Wright, 1967). The unconsolidated uppermost sediments (SUR-19-01) were collected using a rod-operated, wide-diameter Perspex soft-sediment piston corer. The top 1.57 m long SUR-19-01 core was extruded and sub-sampled in the field at 5 mm intervals. The Bolivia cores were split longitudinally using the GEOTEK core splitter at the Australian Nuclear Science and Technology Organisation (ANSTO) facility in Sydney. One-half of the split cores were sub-sampled at 0.5 cm intervals in the laboratory at the University of Adelaide. All untreated sediment samples were stored in sealed polyethylene bags at 4 °C (Dharmarathna, 2022).

2.3. Core correlation and development of a composite record

Sediment cores were photographed and 3D photogrammetric images were derived to remove photographic biases (Ankor and Tyler, 2022). The major element composition of the Bolivia core sediments was measured using an ITRAX μ-XRF scanner (Croudace et al., 2006) at ANSTO and the discrete SUR-19-01 sediments were measured using an Olympus Delta™ handheld X-ray Fluorescence (XRF) analyser at the University of Adelaide. ITRAX inferred element concentrations were calibrated against quantitative XRF analyses on 20 discrete samples chosen from representative locations along the core. Calcium concentration was used as an indicator of calcium carbonate concentration within the sediment, which has previously been described as fine, white laminations throughout the sediment profile (Dharmarathna, 2022). The discrete sample Ca concentration shows a strong correlation ($R^2 = 0.96$) with the ITRAX-inferred Ca averaged across the thickness of each discrete sample, indicating the validity of quantitatively inferring Ca concentration from the ITRAX data. In addition to the diatom analysis data previously published by Barr et al. (2014), 27 samples from SUR-19-01 were analysed for diatoms using the standard methodology explained in Battarbee et al. (2001) and Barr et al. (2014) (Appendix, Fig. A1). A composite sediment stratigraphy was developed by comparing geochemical and visible sedimentary features using the QAnalySeries v.1.5.0 software (Kotov and Pälike, 2018). All depths referred to in this paper are the corrected composite depths.

2.4. ^{210}Pb sediment dating method

^{210}Pb activity was measured on nine samples of approximately 0.5–1 g of freeze-dried sediment from the SUR-19-01 core, covering a total depth of 107.4 cm. All sample preparation and analyses were undertaken at the ANSTO facility in Sydney. Weight measurements taken before and after the freeze-drying process were used to determine the sediments' moisture content and the dry bulk density (Equation (1)).

$$\rho = \frac{S_{wm}}{S_{wv}}\left(1 - \frac{\theta_s}{100}\right) \quad (1)$$

Where, ρ = Dry bulk density (g/ml), S_{wm} = Sample wet mass (g), S_{wv} = sample wet volume (m^3), θ_s = sample moisture content (%).

^{210}Pb remains chemically stable within sediments and decays via beta emission to ^{210}Bi, with a half-life of 22.3 years. Due to the low energy released during this decay process, directly measuring ^{210}Pb is challenging (Nittrouer et al., 1979). Instead, the supported ^{210}Pb activity is measured through its grandparent ^{226}Ra isotope, and the unsupported ^{210}Pb activity is then calculated by subtracting the supported component from the total ^{210}Pb activity, which is measured using its decay product ^{210}Po (Harrison et al., 2003; Hollins et al., 2011; Kosnik et al., 2015). Sediments were prepared for ^{226}Ra and ^{209}Po isotope analyses following the method explained in Harrison et al. (2003). Each Po and Ra source was analysed by high-resolution alpha spectrometry. The chemical yield of ^{226}Ra was determined by measuring the artificial tracer ^{133}Ba on a High Purity Germanium (HPGe) gamma detector. A blank sample of mixed Po and Ba tracers was processed along with the samples. Independent sediment ages and mass accumulation rates were calculated using the CRS and CFCS models (Appleby and Oldfield, 1978).

2.5. Plutonium isotope measurements

Pu isotope concentrations (^{239}Pu, ^{240}Pu and ^{241}Pu) were measured in ten samples extracted at 3 cm intervals of the upper 40 cm of the SUR-19-01 core. Sample processing was carried out in a laboratory with positive-pressure HEPA-filtered air at ANSTO. Approximately 1g of freeze-dried sediment was combusted at 800 °C for 30 min and spiked with ~0.09 pg of NIST SRM 4334 G ^{242}Pu as in isotope dilution reference isotope (Child et al., 2008). Ashed samples were digested with aqua regia solution (3:1 HCl: HNO_3) then dissolved in 3M HNO_3 and processed using ion-exchange chromatography for Pu separation and purification. Pu isotopes were measured using the VEGA Accelerator Mass

Spectrometry (AMS) facility at ANSTO following the methods described in Child et al. (2008) and Hotchkis et al. (2019).

2.6. Radiocarbon dating methods

2.6.1. Pollen sample preparation and analysis

The pollen processing procedure for radiocarbon samples followed a modified method; Acid-alkali-acid (AAA) pollen separation method of Turney et al. (2021) and Cadd et al. (2022) at the Chronos ^{14}Carbon--cycle facility at the University of New South Wales. Samples (5–10 g of wet sediment) were dispersed in 18 MΩ Milli-Q water before passing through a 100 μm sieve. Samples were initially treated with 1 M HCl, heated at 80 °C for 45 min and sieved gently through a 70 μm sieve. 1 M NaOH was added to each sample (material <70 μm) and heated for 30 min at 80 °C. Substantial amounts of extraneous organic material were visible in the pollen samples after NaOH treatment; therefore, samples were treated with saturated KCO_3 and concentrated HNO_3 (Schultz solution) for an hour at 60 °C to eliminate extraneous organic material (Riding, 2021).

Samples were density-separated using sodium polytungstate at a specific gravity of 1.8 g cm^{-1}. The resultant float was sieved through a 20 μm sieve and the material retained on the sieve was transferred to a clean glass centrifuge tube. A second treatment with Schultz solution was conducted to remove any leftover organic matter from the sample. Samples were repeatedly rinsed until a clear supernatant was observed. Finally, 1 M HCl was added to each sample and heated for 1 h at 80 °C. Blank sediment samples (from MIS5 peat sediments; Forbes et al., 2021) were processed alongside the Lake Surprise pollen samples to monitor contamination and for background correction (Turney et al., 2021; Cadd et al., 2022). A total of 10 background (dead C) sediment samples underwent pollen processing and were measured alongside the Lake Surprise pollen samples. The mean F^{14}C of these background samples was 0.0029 ± 0.0001. All pre-treated pollen samples were graphitised with an AGE3 system (Ionplus, Switzerland), where they were combusted in an Elemental Analyzer, with the resulting CO_2 passed through a zeolite trap and subsequently reduced to graphite using hydrogen and an iron catalyst (Wacker et al., 2010; Turney et al., 2021; Cadd et al., 2022). ^{14}C measurements were performed on a MICADAS (Ionplus, Switzerland) Accelerator Mass Spectrometer (AMS) following Turney et al. (2021).

2.6.2. Macrofossil and bulk sediment sample preparation and analysis

During the sub-sampling procedure, samples of macrofossils (leaves, seeds, and twigs) were extracted from all sediment cores using clean, stainless-steel forceps. Bulk sediment was sampled from depths that corresponded with macrofossil samples. Cleaned macrofossils were stored in distilled water before being sent to ANSTO for radiocarbon dating. Samples were pre-treated using the standard acid-alkali-acid (AAA) method to remove carbonates and any contaminating material from the samples (Hua et al., 2001; Norris et al., 2020). All samples were then combusted to CO_2 in a sealed combustion tube, after being dried for approximately 24 h (Hua et al., 2001; Howarth et al., 2013). ^{14}C analysis was undertaken at the ANSTO AMS facility using the techniques described in Fink et al. (2004). ^{14}C values were corrected for the isotope fractionation using ^{13}C measurements obtained from graphite sub-samples using continuous flow isotope ratio mass spectrometry (CF-IRMS) (Fink et al., 2004; Howarth et al., 2013). All radiocarbon dates were calibrated to calendar years using the Southern Hemisphere radiocarbon calibration curve, SHCal 20 for pre-bomb samples and Bomb SH 1–2 data for post-bomb samples (Hogg et al., 2020; Hua et al., 2022). All radiocarbon dates are presented with 1σ uncertainty and ages are reported as calibrated ages before present (cal yr BP).

2.7. Age-model development

The composite age model for Lake Surprise was developed in R using the Bayesian *Plum* model approach (Blaauw and Christen, 2011; Aquino-López et al., 2018). In this study, radiocarbon data from 33 pollen samples and 17 macrofossil samples, the ^{210}Pb activity data and the maximum Pu concentration were utilised to develop the age model (Appendix, Tables A3 and A4). The surface depth, equivalent to the date of sampling (CE, 2019.5), was taken as the uppermost chronological control point. To balance the chronological precision, the model was run in R with relatively higher (8000) iterations and 8 cm thickness while other settings remained as default. The age model was run in R 4.1.3. Software (R Core Team, 2022).

2.8. Contamination screening of pollen extracts using fourier transform infrared (FTIR) analysis

Pollen concentrate radiocarbon samples were screened using the FTIR spectrometry (PerkinElmer Spectrum 400 FTIR) using the attenuated total reflectance (ATR) mode to identify any non-pollen contaminants such as inorganic carbonate, charcoal and other organic residues (Appendix, section 3). Only the samples dated above ~3 m (8 samples) were able to be screened using FTIR because the remaining material of the bottommost samples were insufficient to obtain an accurate spectrum (Appendix, Table A6). The transmittance (T) spectrum was converted to absorption (A), using equation $A = 2 - \log_{10}(T)$, and a linear baseline correction was applied before further data analyses. The values were expressed in percentage of total absorbance.

3. Results

3.1. Lake sedimentology

The analysed sediments consistently showed a fine, clay-rich texture with blackish grey in colour, except for the bottommost sediments (lower depths of SUR-19-02 and SUR-19-03), which were marginally coarser-grained (Dharmarathna, 2022). Undisturbed, fine laminations were observed throughout the sediment depths of SUR-19-02 and SUR-19-03 (Appendix, Fig. A2). More detailed, high-resolution images of these cores were captured and analysed by Ankor & Tyler (2022) using a computational photography method.

3.2. Results of ^{210}Pb activity measurements

The unsupported ^{210}Pb activity values were significantly higher (5–901 Bq kg^{-1}) than the supported ^{210}Pb activities (3.4–4.8 Bq kg^{-1}) and contributed most to the total ^{210}Pb activity profile (Table 1).

The total and unsupported ^{210}Pb activity profiles illustrate decreasing trends with depth (Fig. 2a), with unsupported ^{210}Pb activity reaching its measurable background at 107.4 cm (5 ± 1 Bq kg^{-1}). Two preliminary CFCS and CRS age models were derived using ^{210}Pb activity alone, according to which the age at 107.4 cm from the CFCS age model is comparatively older (152 ± 18 years) than the CRS age model (128 ± 10 years) (Fig. 2b). The CFCS age model was calculated from two sets of constant mass accumulation rates for lower and upper zones as 0.077

Table 1
^{210}Pb activity in the SUR-19-01 sediments.

Depth range (cm)	Mid-point depth (cm)	Supported activity (Bq/kg)	Unsupported/ excess activity (Bq/kg)	Total activity (Bq/kg)
0–1.4	0.7	4.8 ± 1.0	901 ± 47	906 ± 47
8.4–9.8	9.1	3.8 ± 0.7	715 ± 35	719 ± 35
16.8–18.2	17.5	4.3 ± 0.6	249 ± 11	253 ± 11
25.2–26.6	25.9	5.1 ± 0.7	164 ± 8	170 ± 8
40.9–42.0	41.5	3.3 ± 0.6	32 ± 2	35 ± 2
53.8–54.8	54.3	3.3 ± 0.5	15 ± 1	18 ± 1
65.8–66.8	66.3	2.7 ± 0.4	15 ± 1	17 ± 1
86.3–87.5	86.9	2.3 ± 0.3	7 ± 1	9 ± 1
106.8–107.8	107.4	3.4 ± 0.5	5 ± 1	9 ± 1

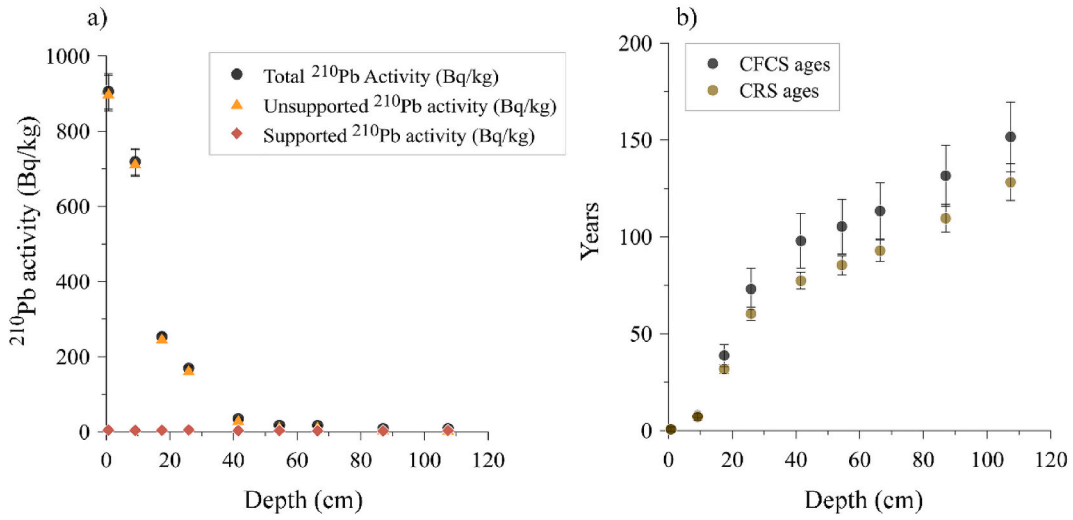

Fig. 2. a) ^{210}Pb activity profile and b) calculated CFCS and CRS ages versus sediment depth. Depth in the X-axis refers to the corrected composite depth.

and 0.0196 gcm^{-2}/year, respectively (Appendix, Table A1). The sediment accumulation rate is considerably higher and more variable in the CRS age model with values varying from 0.018 to 0.098 gcm^{-2}/year. Both models suggest a significant increase in accumulation rate from around 30–40 cm (Fig. 2b).

3.3. Plutonium isotope measurements

The total Pu concentration varied from 0.02 to 1.30 pg/g (Fig. 3a; Appendix, Table A2). Pu isotope concentration in the sediments decreased in the order of ^{239}Pu, ^{240}Pu and ^{241}Pu, with values of ^{239}Pu and ^{240}Pu measured above the background level, with values ranging from 0.02 to 1.11 pg/g for ^{239}Pu and 0.003–0.190 pg/g for ^{240}Pu

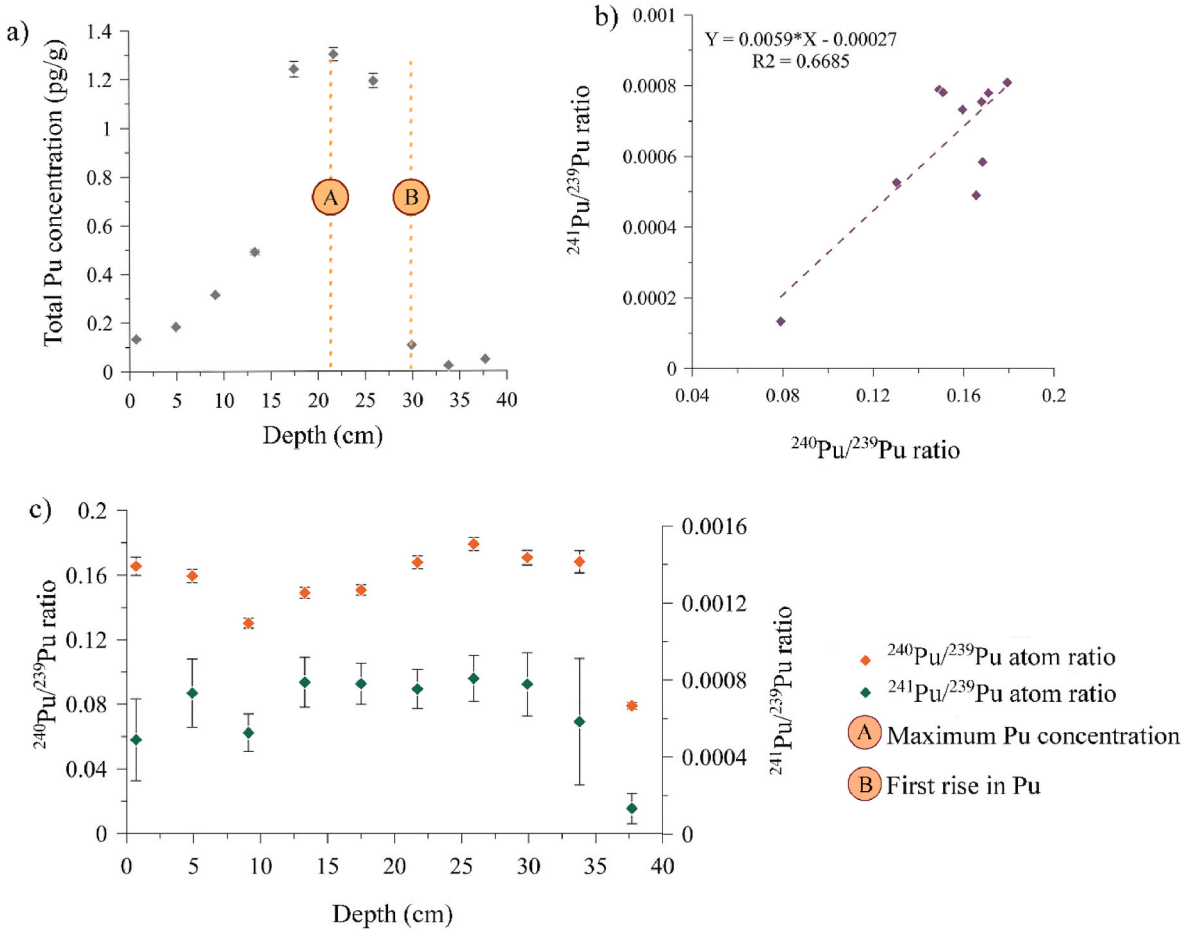

Fig. 3. a) Total Pu concentration b) linear correlation between $^{240/239}$Pu and $^{241/239}$Pu atom ratios and c) representation of Pu isotope ratios against sediment depth. Depth in the X-axis refers to the corrected composite depth.

(Appendix, Table A2). The two bottom samples illustrate much lower Pu concentrations, with their values being approximately three orders of magnitude higher than the average value of chemistry blanks (0.01 fg for ^{239}Pu and 0.001 fg for ^{240}Pu and ^{241}Pu) (Appendix, Table A2). $^{239+240}$Pu values of these sediments ranged from 0.07 to 4.13 mBq/g. ^{240}Pu/^{239}Pu atom ratios represent relatively higher values (0.08–0.18) compared to the ^{241}Pu/^{239}Pu ratio (Fig. 3c), in which values ranged from $1.33*10^{-4}$ – $8.09*10^{-4}$ (Appendix, Table A2).

Sediments exhibit elevated total Pu concentration levels in samples ranging from 17.5 to 25.9 cm, reaching a peak at the depth of 21.7 cm (1.30 pg/g; Fig. 3a). The major increase in Pu commenced at 29.9 cm, and values remained high until 17.5 cm, after which they began to decline progressively towards the surface (Fig. 3a). Atom ratios of $^{240/239}$Pu and $^{241/239}$Pu remained nearly consistent at around 0.13–0.18 and $4.90*10^{-4}$ – $8.09*10^{-4}$ respectively, except for the bottommost (older) sample at 37.7 cm, which consists of much lower values of 0.079 and $1.33*10^{-4}$ in respective order (Fig. 3b). A moderate to strong linear correlation ($R^2 = 0.67$) is observed between $^{240/239}$Pu and $^{241/239}$Pu atom ratios (Fig. 3b).

3.4. Radiocarbon dating

Macrofossil samples measured at depths of 15.05 cm and 31.55 cm illustrate a peak in ^{14}C content (pMC ≥135), with ^{14}C ages recorded as −13 ± 3 and −22 ± 3 respectively (Table 2a). These modern ^{14}C samples represent 1972 ± 3 and 1963 ± 3 in calendar years (CE). Radiocarbon ages show stratigraphic consistency throughout the core, with the lowermost pollen age at 1132.5 cm returning to a ^{14}C age of 10034 ± 20 (Table 2b).

There is an age reversal in the radiocarbon dates of macrofossil samples dated at 566 cm and 615 cm, with the shallower date (OZZ-524) being older than the deeper date (OZZ-523) (Table 2a; Fig. 4). Similarly, the pollen sample dated at 643.5 cm (UNSW 514) represents younger age compared to other pollen radiocarbon ages (Table 2b). The pollen concentrates found both above and below this depth represent a relationship of increasing age with depth. The presence of undisturbed fine laminations throughout the core depths indicates the absence of macrofossil re-deposition or movement, as well as any slumping within the sediment profile (Appendix, Fig. A2). Macrofossil samples dated in this study are seed pods, bark or twig fragments and leaves. It is highly unlikely that younger plant material such as roots penetrated into older sediment. Therefore, we can rule out the contamination by younger carbon in this setting. Further, given that the "age reversal" is only evident in a single macrofossil and a pollen sample, this can either be regarded as a contamination or an outlier. Therefore, OZZ 523 and UNSW 514 were manually removed prior to the final age-model run.

Table 2b
Radiocarbon ages of pollen fraction from Lake Surprise sediment cores analysed in this study. Calibrated ages were calculated using the SHCal 20 calibration curve (Hogg et al., 2020).

Material dated	Depth (cm)	Lab ID	^{14}C age		Unmodelled (BP), 95.4 %	
			Mean	1σ	From	to
Pollen	41.2	UNSW-490	314	20	442	291
Pollen	52.15	UNSW-491	375	20	487	320
Pollen	62.15	UNSW-492	387	20	491	323
Pollen	73.45	UNSW-493	423	20	499	331
Pollen	77.65	UNSW-497	451	20	505	338
Pollen	97.3	UNSW-494	475	20	522	466
Pollen	104.45	UNSW-526	565	20	552	512
Pollen	116.65	UNSW-495	581	20	623	516
Pollen	136.45	UNSW-496	865	20	767	680
Pollen	151.51	UNSW-499	939	20	904	735
Pollen	188	UNSW-500	1666	20	1579	1427
Pollen	218	UNSW-501	1549	20	1425	1315
Pollen	253	UNSW-502	1760	20	1700	1569
Pollen	274.5	UNSW-503	2026	20	1999	1887
Pollen	310.5	UNSW-504	2424	20	2677	2341
Pollen	348.5	UNSW-505	2537	20	2729	2439
Pollen	407.5	UNSW-506	2862	20	3057	2851
Pollen	450	UNSW-507	3291	20	3560	3393
Pollen	479	UNSW-530	3329	20	3572	3450
Pollen	509.5	UNSW-510	3442	20	3818	2571
Pollen	541.5	UNSW-511	3525	20	3844	3648
Pollen	579	UNSW-512	3976	20	4516	4251
Pollen	608.5	UNSW-531	3984	20	4519	4256
Pollen	643.5	UNSW-514	3549	20	3877	3695
Pollen	717.5	UNSW-516	4785	20	5584	5329
Pollen	809	UNSW-517	5682	20	6494	6315
Pollen	854.5	UNSW-518	6625	20	7566	7427
Pollen	924	UNSW-519	6847	20	7688	7584
Pollen	956	UNSW-520	7428	20	8333	8040
Pollen	982	UNSW-521	7408	20	8320	8035
Pollen	1016	UNSW-522	8049	20	9009	8725
Pollen	1056.5	UNSW-524	8658	20	9679	9533
Pollen	1132.5	UNSW-523	10034	20	11627	11465

Table 2a
Radiocarbon ages of macrofossil and sediment samples from Lake Surprise sediment cores analysed in this study. Calibrated ages were calculated using the SHCal 20 calibration curve (Hogg et al., 2020).

Material dated	Depth (cm)	Lab ID	δ^{13}C (‰PDB)	^{14}C content (pMC)		^{14}C age		Sediment-macrofossil age offset (^{14}C yr)		Unmodelled age (cal. BP) 95 %	
				Mean	1σ	Mean	1σ	Mean	1σ	from	to
Plant	15.05	OZZ426	−28.7	135.66	0.35	−13	3			−10	−30
Plant	31.55	OZZ427	−28.7	147.88	0.40	−22	3			−11	−25
Macrofossil	96.2	OZZ429	−28.6	96.89	0.24	255	20			304	151
Macrofossil	129.3	OZZ514	−25.7	94.44	0.26	460	22			512	339
Sediment	129.3	OZZ515	−29.8	91.73	0.24	693	21	234	31	536	501
Macrofossil	136.45	OZZ430	−28.0	93.65	0.20	525	20			538	500
Plant	214	OZZ516	−28.8	85.46	0.19	1262	18			1256	1066
Sediment	214	OZZ517	−27.7	81.80	0.22	1614	22	352	26	1530	1380
Plant	288	OZZ518	−28.3	79.35	0.22	1858	22			1826	1639
Sediment	288	OZZ519	−29.1	77.82	0.23	2014	24	156	33	1999	1840
Macrofossil	375.5	OZZ521	−25.3	74.81	0.20	2331	21			2352	2151
Plant	379.5	OZZ520	−28.3	75.71	0.23	2235	24			2324	2106
Plant	497	OZZ522	−29.0	68.06	0.18	3091	21			3356	3171
Plant	566	OZZ524	−28.4	61.80	0.15	3866	20			4402	4097
Macrofossil	615	OZZ523	−28.0	64.18	0.16	3562	20			3891	3700
Plant	744.5	OZZ525	−27.0	55.19	0.16	4775	23			5583	5327
Plant	776.5	OZZ526	−28.6	53.47	0.16	5029	24			5890	5602
Macrofossil	782.5	OZZ527	−29.1	52.84	0.15	5124	23			5914	5813
Plant	898	OZZ528	−26.4	45.66	0.14	6297	25			7265	7020
Sediment	898	OZZ529	−35.3	44.32	0.14	6537	25	239	35	7482	7321

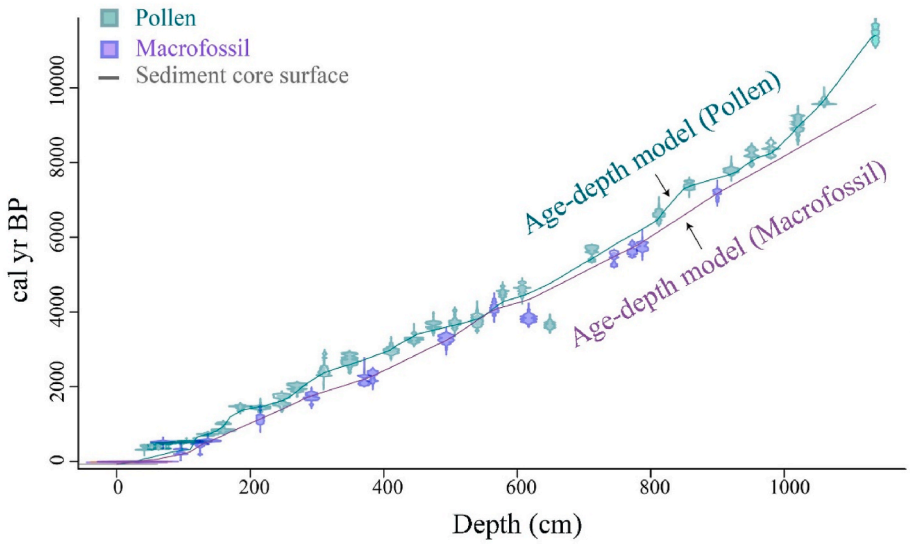

Fig. 4. Radiocarbon dates of pollen (Table 2b) and macrofossil (Table 2a) samples against sediment depth. Green and purple lines represent the mean value of Bacon age-depth models developed using only these radiocarbon data.

Age offsets (differences in ^{14}C ages) are observed between bulk sediment and macrofossil samples for the same depths, with the bulk sediment showing older ages compared to the macrofossils. These offsets range from 156 ± 33 to 353 ± 26 with a weighted mean value of 260 ± 86 years (Table 2a). When comparing modelled ages based solely on pollen dates, vs. those derived from macrofossil dates, it is apparent that pollen dates are noticeably older than the macrofossil dates throughout the sediment depth (Fig. 4). This age offset is evidenced at 136.45 cm, where pollen and macrofossil dates have an age offset of ~340 years (Table 2a & 2b). This offset cannot be compared in the bottommost section of the core (~900–1100 cm), due to the absence of any macrofossil dates. When this age offset is plotted against sediment depth, it appears that parts of the core when the age offset is greatest correspond with high carbonate concentration, as indicated by ITRAX-inferred calcium concentration, albeit with some inconsistencies (Fig. 5). The lower age-offset around 250 cm, which corresponds with high Ca% and higher age-offset at around 300 cm, where Ca% remains low are such inconsistencies. Similarly, the increasing trend of age offset from around 550 to 800 cm aligns with low Ca%. These differences suggest that while the processes affecting carbonate deposition and radiocarbon age offset are possibly related, there is no definitive relationship.

3.5. FTIR screening of pollen purity

FTIR spectroscopy has long been used as a fast and cost-effective technique to determine the molecular structure of organic and inorganic components of lacustrine sediments (Korsman et al., 2005; Rosan and Hammarlund, 2007; Liu et al., 2013; Maxson et al., 2021; Ninnes et al., 2024). FTIR analysis is based on the principle that absorption of IR radiation by a molecule triggers vibrations in covalent bonds, with each occurring at specific wavenumbers in the IR spectrum. These absorption patterns correspond to specific chemical bonds or functional groups. The intensity of absorption can be assessed using either reflectance or transmittance methods across a broad range of wavelengths (Toffolo, 2025; Rosén et al., 2010; Chen et al., 2015). The commonly studied wavelength range is in the mid-IR range (4000–400 cm^{-1}). Although this is a highly precise technique, interpreting IR spectra can be difficult, particularly due to overlapping bands, where functional groups of different molecules absorb IR radiation at similar frequencies(Liu et al., 2013; Maxson et al., 2021; Ninnes et al., 2024).

FTIR spectra of analysed pollen concentrate samples are shown in Fig. 6. The major bands of absorption spectra are centred on wavelengths of 1000 cm^{-1}, 2800–3000 cm^{-1} and ~1500–1700 cm^{-1}, along with a broader stretching band at around 3200–3600 cm^{-1} (Fig. 6). The very strong narrow bands centred around 1000 cm^{-1} (900–1200 cm^{-1})

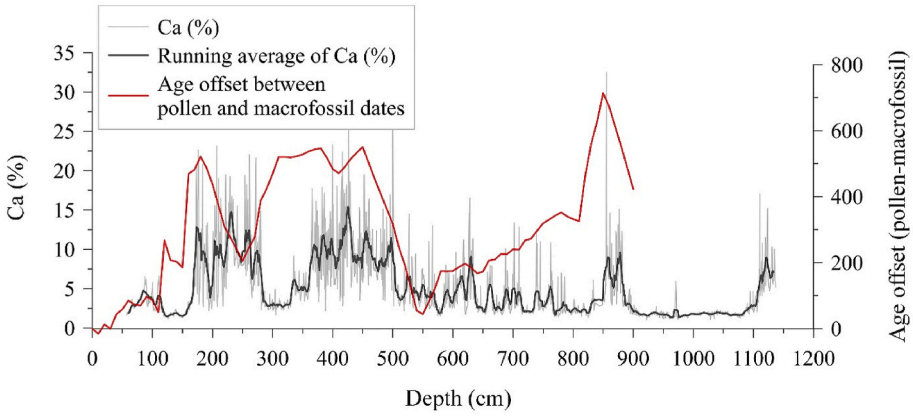

Fig. 5. Comparison of age offset between pollen and macrofossil dates against measured Ca (%) values through the sediment depth. The black line represents the moving average of the 15-width range for Ca data (Appendix, Table A7).

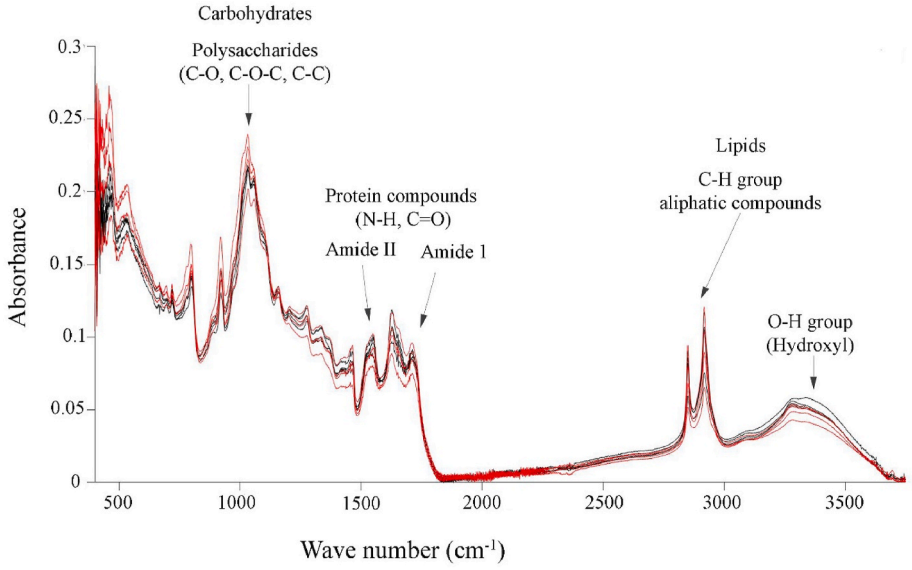

Fig. 6. FTIR absorption spectrum of eight radiocarbon-dated pollen samples from above 3 m depth. The red-coloured spectra are samples with higher age offset (>300 cal yr BP) and black spectra indicate samples with lower age offset (≤200 cal yr BP). Refer to Appendix, Table A6 for their sediment depths and age-offset values. (Jebsen et al., 2012; Liu et al., 2013).

represents polysaccharide groups that are composed of various C – O and C – O – C, C – C and C – P bonds (Jebsen et al., 2012; Abdala Díaz et al., 2019; Hong et al., 2021). Relatively strong absorption bands observed around 2800–3000 cm^{-1} from C – H stretching show that the majority of the organic matter in the pollen is aliphatic, with little or no signal between 3000 and 3100 cm^{-1}, characteristic of C – H stretching from aromatic organic material (Jebsen et al., 2012; Liu et al., 2013). Moderate bands that spread from 1500 to 1700 cm^{-1} mainly represent protein group compounds of amide I and II that consist of N – H and C – N bonds (Mecozzi et al., 2009; Jebsen et al., 2012; Liu et al., 2013). The broad band observed after 3000 cm^{-1} indicates the presence of hydrogen-bonded hydroxyl groups (O – H) and carboxylic acids (COOH), which are a commonly observed functional group in all proteins, lipids and carbohydrates (Kovac et al., 2005; Liu et al., 2013). Carbonate bands are not identifiable in the FTIR spectrum (~900 and ~1435; Fig. 6). In addition, there are a few other small-moderate peaks, the source of which is unidentified. The spectra show a strong similarity indicating that the protein, carbohydrate and lipid fractions known to make up pollen are very similar in each sample.

4. Discussion

4.1. Interpretation of ^{210}Pb activity in lake surprise sediments

The unsupported ^{210}Pb activity profile (Fig. 2a) in Lake Surprise sediments demonstrates a steady (monotonic) decline, suggesting that the unsupported ^{210}Pb accumulation rate is most likely to be uninterrupted by external processes like burial, removal of organic matter and dilution of ^{210}Pb by increased rates of sediment accumulation (Appleby, 2001; Holmgren et al., 2010). In contrast, the estimates from the CFCS model show two variations in the sediment accumulation rate (Appendix, Table A1), suggesting the occurrence of potential minor changes in sedimentation rate over time (Appleby, 2001; Harrison et al., 2021). However, it is also identified that such deviations may occur due to multiple other natural reasons such as the availability of a zone of incomplete mixing close to the surface or radioisotope migration through sediments (Benoit and Rozan, 2001; Harrison et al., 2021). Deviations in modelled accumulation rate can also be caused artificially, where sediment accumulation rates tend to vary due to the mathematical framework used in CRS/CFCS modelling (Aquino-López et al., 2020a). Given that Lake Surprise is in a relatively sheltered catchment, it is feasible that sedimentation rates were relatively constant over the last century. However, the analysis of sediment samples from core SUR-19-01 reveals high water content and an absence of visible laminations (in contrast to the deeper lake sediments), suggesting a potential for sediment mixing either at the sediment-water interface or during the coring process.

4.2. Interpretation of Pu isotopes for lake surprise chronology

The transfer of plutonium from the Northern Hemisphere (NH) as a result of nuclear testing to the Southern Hemisphere (SH) took approximately one to two years (Leslie and Hancock, 2008; Hancock et al., 2011). Even though the Lake Surprise data show a broader peak, the highest Pu concentration observed at 21.7 cm can be matched with the maximum SH Pu fallout recorded ~1964 following the US/former USSR nuclear tests in 1962–1963 (Hancock et al., 2011; Hirose and Povinec, 2015; Harrison et al., 2021). The $^{240}Pu/^{239}Pu$ atom ratio in Lake Surprise provides indications of both the global and local inputs of Pu into the sediment (Thakur et al., 2017; Harrison et al., 2021). The oldest sample (measured at 37.7 cm) with a relatively low $^{240}Pu/^{239}Pu$ atom ratio is likely to have a different origin, given that it deviates from all other samples, which plot within or near the range of SH atmospheric fallout values (0.185 ± 0.014) (Fig. 3b & c) (Kelley et al., 1999). This is consistent with the significantly lower $^{240}Pu/^{239}Pu$ atom ratios seen in nuclear tests conducted at Australian sites in the early 1950s (such as Emu Field, Maralinga, and Montebello Islands; <0.07) (Child and Hotchkis, 2013; Smith et al., 2016; Harrison et al., 2021). It is suggested that during the pre-moratorium period (1952–1954 CE), high $^{240}Pu/^{239}Pu$ atom ratios resulted from atmospheric fallout, particularly when US-dominated testing released more than 90 % of the global fallout (Koide et al., 1982; Muramatsu et al., 2001; Harrison et al., 2021). This aligns with the interpretation that the oldest sample may have originated from a local Pu source. Several other Australian studies have also reported low $^{240}Pu/^{239}Pu$ atom ratios and have proposed a similar influence (Everett et al., 2008; Tims et al., 2013; Johansen et al., 2016).

The second major Pu chronological marker used is the period of the first detection of Pu, signifying when there was enough cumulative activity in the sediment to be detected (Leslie and Hancock, 2008).

Previous studies from Australia and elsewhere have shown that detectable Pu fallout initially occurred in the southern latitudes (30°–40°S) in 1954 (Leslie and Hancock, 2008; Hancock et al., 2011, 2014; Harrison et al., 2021). While all the measured samples exceeded the detectable limit of Pu for the AMS technique, the bottommost sample has a $^{240}Pu/^{239}Pu$ ratio of 0.079 ± 0.002 (Appendix, Table A2), which is lower than the global fallout range of 0.16–0.19 (global average = 0.18) and even below the previously recorded range for Victoria (~0.12–0.20) (Krey et al., 1976; Tims et al., 2013). Similarly, measured low concentrations near background levels of total Pu and $^{239+240}Pu$ at 33.8 cm further suggest that the two bottommost samples are likely to represent the period before the first detectable limit of global Pu fallout (Appendix, Table A2). Therefore, it is likely that the first detection of fallout Pu (~1954) at Lake Surprise was recorded at 29.9 cm, along with the initiation of the steep rise in Pu concentration in the sediment (Fig. 3a). Higher Pu content observed immediately before and after the maximum Pu content may represent the influence of former Soviet Union tests (1961–1962) and French testing in the South Pacific (1964–1974), in addition to United States-dominated global fallout (UNSCEAR, 2000; Hirose and Aoyama, 2003). Therefore, it is apparent that Lake Surprise sediments may illustrate a combination of global and local Pu fallout, characterised by high and low $^{240}Pu/^{239}Pu$ atom ratios. This is justified by the relatively broad Pu profile near the maximum (Fig. 3a), which may occur due to the amalgamation of different Pu sources (Harrison et al., 2021). Overall, the total Pu content in lake sediments follows the global fallout pattern, high from the 1960s to early 1970s, then declining post-1980 due to reduced atmospheric testing (Hancock et al., 2011; Harrison et al., 2021).

4.3. Age offsets between bulk sediment, pollen grains and macrofossils

Comparison between radiocarbon macrofossil ages with pollen extract and bulk sediment ages indicate the presence of 'old' carbon in both pollen and bulk sediments (Table 2a and Fig. 4 for C^{14} ages). The old carbon effect, where contemporaneous ^{14}C-rich material is mixed with carbon from ^{14}C-depleted or 'old' contaminants is a common feature in western Victorian lakes, due to their carbonate-rich (limestone) geological setting (Price et al., 1997; Wilkins et al., 2012). Old carbon can also be assimilated into organic matter, via lacustrine algae utilising carbon derived from groundwater or dissolved carbonates (Mazumder et al., 2019). In stratified lakes, reduced mixing rates may deplete the ^{14}C reservoir in the water column compared to atmospheric CO_2 (Philippsen, 2013; Zhou et al., 2015, 2020; Schneider et al., 2019). A previous study from Lake Surprise found an age offset between pollen grains and bulk sediment of 424 ± 75 ^{14}C years (Barr et al., 2014). Groundwater-derived 'old' carbon may explain the offset between the bulk sediment and terrestrial macrofossil ages (Barr et al., 2014) but would not account for the offset between macrofossil and pollen concentrate, if the latter derived from pure terrestrial pollen.

Explaining old pollen radiocarbon ages is complicated since terrestrial pollen assimilates atmospheric CO_2 equivalent to terrestrial macrofossils. Despite this, several previous studies have reported pollen radiocarbon ages older than the sediment's depositional age (Kilian et al., 2002; Howarth et al., 2013; Fletcher et al., 2017; Martin et al., 2019; Zimmerman et al., 2019; Schiller et al., 2021). So far, multiple hypotheses have been proposed to explain the relatively old pollen ages, including contamination of pollen grains by micro-charcoal or other organic remains (algae, spores) (Martin et al., 2019; Kilian et al., 2002; Fletcher et al., 2017) and the fluvial reworking of pollen from watershed soils or older exposed lake sediments (Howarth et al., 2013; Zimmerman et al., 2019), which may outnumber pollen grains (Gell et al., 2005). The Flow Cytometry method has been shown to overcome some these challenges, particularly in purification and obtaining sufficient quantities of pollen grains for ^{14}C dating (Tennant et al., 2013; Zimmerman et al., 2019; Kron et al., 2021; Tunno et al., 2021). However, its effectiveness when applied to different sedimentary sequences remains largely untested (Tennant et al., 2013; Zimmerman et al., 2019; Tunno et al., 2021). Despite these various pollen concentration techniques developed over time, achieving complete purification remains a challenge (Zimmerman et al., 2019; Cadd et al., 2022). The incomplete removal of organic/inorganic matter from pollen concentrates is identified as the main cause of carbon contamination in pollen concentrate ages (Long et al., 1992; Tennant et al., 2013; Zimmerman et al., 2019; Tunno et al., 2021; Cadd et al., 2022).

In the sediments of Lake Surprise, despite some inconsistencies, there is a general correspondence between the pollen-macrofossil age offset and carbonate concentration (indicated by Ca%; Fig. 5). The correspondence between ^{14}C offset and sediment carbonate concentration suggests that old carbon derived from carbonate-rich groundwater may be partly responsible, either through direct carbonate contamination of the sediment or indirectly via incorporation in aquatic organic matter. Contamination of pollen extracts via direct calcium carbonates can be largely eliminated as a potential explanation. Firstly, the pollen grains were treated twice in concentrated acids (HCl) for ~45 min and it is unlikely that calcium carbonates were retained through this treatment. This is further confirmed by FTIR analysis, which indicates the absence of any absorption bands corresponding to wave numbers of inorganic carbonate (860–900 cm^{-1} and 1300–1600 cm^{-1}) (Liu et al., 2013) (Fig. 6). Several other studies have suggested that carbonates may form relatively moderate absorption bands at around 700–725 cm^{-1}, ~1800 cm^{-1} and 2500 cm^{-1} due to the C=O bond (Mecozzi et al., 2001; Kovac et al., 2005; Liu et al., 2013), however, none of these bands is apparent in the pollen FTIR data either (Fig. 6). Micro-charcoal is also a common pollen contaminant that may contribute to older ages, particularly in fire-prone environments like south-eastern Australia (Kershaw et al., 2002; Harris et al., 2017; Martin et al., 2019). Although fine charcoal particles were observed throughout the Lake Surprise sediments during the sub-sampling procedure, the FTIR results do not exhibit distinct infrared absorption bands at 1400 cm^{-1} or 1640 cm^{-1} wavelengths commonly associated with charcoal (El-Eswed, 2016). Even though absorption bands corresponding to these wavelengths are present, a significant difference cannot be identified between these spectra to differentiate the presence of charcoal in these sediments (Fig. 6). This does not exclude charcoal contamination for all pollen radiocarbon dates; however, it does suggest that charcoal contamination is only a minor contributor to the age offset. Additionally, the lack of clear separation in the absorption spectra between the samples with larger and smaller age offsets inhibits the identification of the exact pollen contaminant.

Storage of pollen grains in catchment soils and subsequent remobilisation is considered another possibility that could contribute to the age offsets in the pollen samples (Mensing and Southon, 1999; Howarth et al., 2013; Neulieb et al., 2013; Fletcher et al., 2017). However, the steep catchment slopes and likely short residence time of pollen remains accumulating in the topsoil (Timms, 1976; Barr et al., 2014; Falster et al., 2018) discount this hypothesis for the magnitude of age offsets estimated. Reworked pollen grains if present, should appear broken or degraded under a light microscope (Lowe, 1982; Tweddle and Edwards, 2010; Dingemans et al., 2014). However, the well-preserved pollen from this site, coupled with the finely laminated sediments (Ankor and Tyler, 2022) makes the idea of vertical migration of pollen grains even more unlikely.

The remaining possible explanations for 'old' carbon effects in the pollen extracts, therefore, rely on old ^{14}C being included within a pollen-like matrix. A potential explanation is the presence of algae amongst the isolated pollen. Studies elsewhere have suggested that the isolation of aquatic algae from pollen grains is difficult compared to other non-pollen material (Regnéll, 1992; Fletcher et al., 2017; Steinhoff et al., 2022). Aquatic algae have the potential to utilise dissolved inorganic carbon that may be contaminated with ^{14}C-depleted carbon derived from groundwater (Cartwright et al., 2020). Similarly, algae may also consume methane or CO_2 generated by the remineralisation of older

sediments (Zhou et al., 2015). Sediment samples were sieved at 20 μm and density separated at 1.8 g cm^{-1}, but some algal colonies are similar in size and density to pollen grains, making their removal from the pollen matrix challenging. To reduce the contamination by algae, a harsh oxidant, Shultz solution (Riding, 2021), was applied to the samples. Algae (colonial algae and *Botryococcus*) were observed visually during sample processing, but following the pollen isolation, the samples were clumped and dry, making it challenging to detect the presence of aquatic contaminants under a light microscope. *Botryococcus* algae form rich hydrocarbon-rich membranes that are high in carbohydrates and lipids. The FTIR spectra have absorption bands associated with carbohydrates, proteins and lipids, which may suggest the presence of *Botryococcus* algal remains (Jebsen et al., 2012; Liu et al., 2013) (Fig. 6). Overall, the FTIR results suggest that while charcoal and carbonate contamination are unlikely factors, it is feasible that the pollen extracts contained some fraction of algal-derived material, and that this algal matter was influenced by changes in the lake's carbon cycle through time. Feasible explanations for a relationship between carbonate deposition and radiocarbon uptake by algae include uptake of groundwater-derived inorganic carbon, uptake of CO_2 produced by the remineralisation or methanogenesis of older sediments, or due to a change in pH and inorganic carbon speciation arising from changes in lake productivity.

4.4. Chronology for holocene sediments at lake surprise

To account for the age offset in pollen radiocarbon dates, a correction was applied, using a mean age offset of 340 ± 50 years, input as Delta.R and Delta.STD in *Plum* (Appendix, Table A3). The final age model integrated these corrected radiocarbon dates from pollen, along with macrofossil dates, ^{210}Pb activities and the year of maximum Pu concentration.

The upper portion of the final age model was evaluated using independent chronological markers (Fig. 8). These were the first detection of Pu, an age estimate of the *Pinus* pollen arrival at Lake Surprise (75 ± 20 cal yr BP) and the date of the previous sediment coring (core LSFS) (−54 ± 2 cal yr BP; 2004 CE) (Appendix, Table A5). The latter two were identified by comparing the corresponding diatom species composition data counted at 4 cm resolution from SUR-19-01 with the diatom record in Barr et al. (2014) (Appendix, Fig. A1). Accordingly, the top of the LSFS core was estimated to be equivalent to approximately 5 cm depth in SUR-19-01.

Many age markers (both independent markers and those which contributed to the model) plot within the 95 % confidence interval of the modelled ages (Fig. 8) indicating that the final model is acceptable within the given age limits. However, it is worth noting that the CFCS and CRS models, which do not include the *Pinus* arrival date or any ^{14}C data, deviate from the *Plum* model towards older ages with increasing age uncertainties. Previous records have explained this behaviour as an artificial increase in the sedimentation rate due to mathematical structure and differing interpolations used in the model, where the age function tends to reach infinity as a response to the decreasing ^{210}Pb activity (Aquino-López et al., 2020a, 2020b; Barsanti et al., 2020). Given the higher uncertainties, it has been recommended that CFCS and CRS-derived ^{210}Pb ages older than ~100 years be presented as extrapolations instead of directly measured ages (Barsanti et al., 2020). By contrast, *Plum* offers the ability to include additional data, which in turn means that Plum models are less likely to reflect artificial increases in

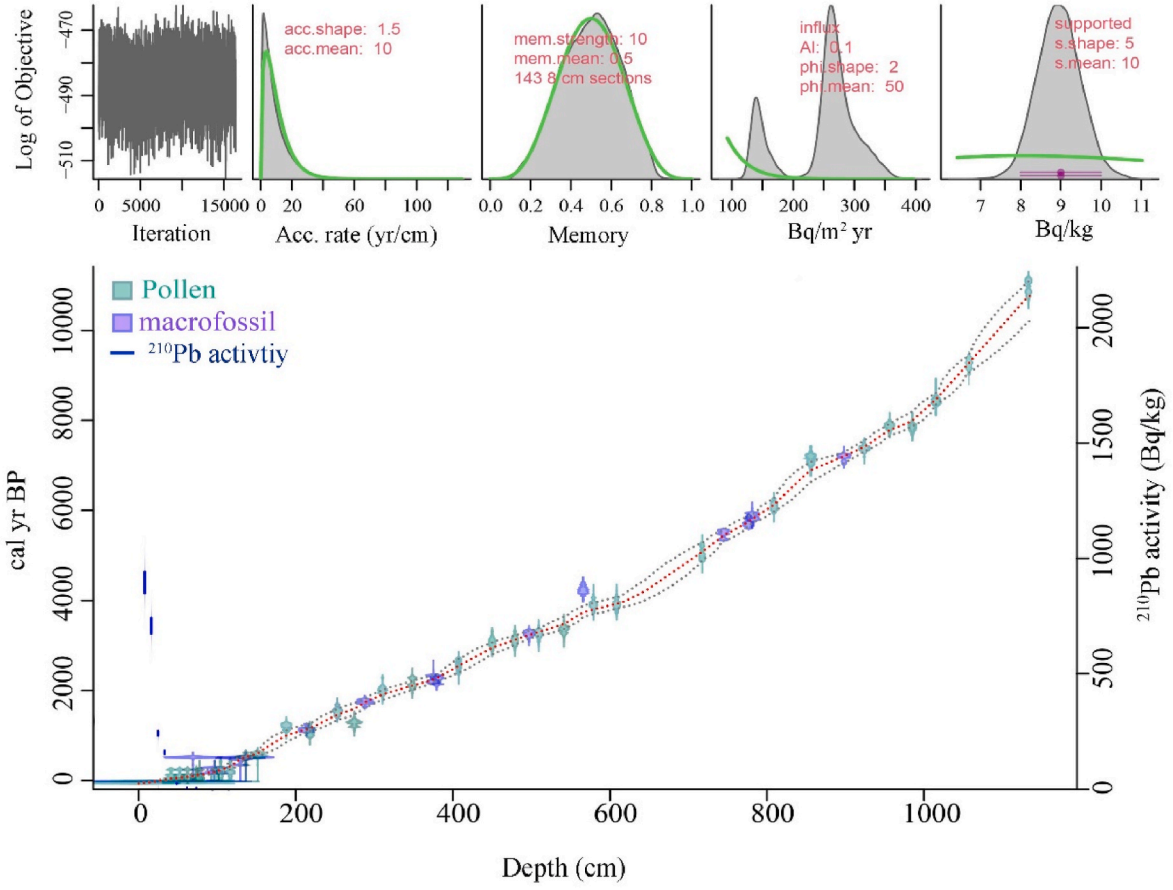

Fig. 7. Lake Surprise age model derived using radiocarbon ages of pollen and macrofossil samples, ^{210}Pb activities and Pu concentration in the *Plum* package in R 4.1.3 software (R Core Team, 2022). All ^{14}C dates were calibrated to SHCal20 (Hogg et al., 2020). The red dotted line represents the mean value (true age-depth function), and the black dotted lines represent the 95 % confidence interval.

sedimentation rate (Aquino-López et al., 2020a). Our comparison of the CRS, CFCS and *Plum* models suggests that *Plum* has a higher potential to capture true ages in the Lake Surprise sediment.

According to the median of the modelled age estimates, the entire sediment profile (~11.37 m) extends to ~10,846.6 ± 900 cal yr BP with a mean sedimentation rate of approximately ~9.5 yr/cm (Fig. 7). A past study from Lake Surprise indicates average sedimentation of <10 yr/cm in the upper 3 m of a previously recovered sediment core (Barr et al., 2014). However, the chronology of this core was developed using CRS modelling of ^{210}Pb dates and a limited number of radiocarbon dates, where linear interpolations were required to estimate the basal age (Barr et al., 2014). However, high sedimentation rates found in this study agree with several other studies that identified continuous and nearly consistent sedimentation of roughly 30,000 cal yr BP, obtained from 30 pollen-derived radiocarbon dates of an ~18 m thick sediment sequence at Lake Surprise (Tibby et al., 2006; Builth et al., 2008; Falster et al., 2018). Even though it is recommended that lake sedimentation should be at least 1m/1000 years to allow a sampling routine that would typically offer a sub-decadal scale temporal resolution per sample, many Australian lake sediment records exhibit a lower sedimentation rate, at least in the period before landscape clearance by European settlers (Harle et al., 2005). However, our interpretation, along with previous studies (Barr et al., 2014; Falster et al., 2018), suggests that Lake Surprise has a suitable rate of sedimentation throughout the entire Holocene to offer the potential for decadal-scale environmental and climate reconstructions.

5. Conclusion

In this study, a well-constrained chronology was developed for the Holocene sediments of Lake Surprise using a combination of ^{210}Pb, radiocarbon and historical markers, including the deposition of anthropogenic radionuclides. The behaviour of the ^{210}Pb profile and the well-resolved structure of the Pu concentration illustrate that sediment mixing or any other physical processes are mostly unlikely. Relatively low Pu concentrations, and lower isotope ratios (^{240}Pu/^{239}Pu) in the early Pu record may indicate the influence of Pu from both the global and local atmospheric fallout. This is further supported by the broader fallout peak in the record. The age model agrees with the majority of the recent chronomarkers demonstrating its accuracy and reliability.

AMS ^{14}C dates were analysed across multiple datable materials to obtain the most reliable chronology. In the pre-modern sediments, the majority of the chronology is based on pollen ages, given the scarcity of sufficient macrofossils from the sediment. An old carbon effect in this study has been estimated using bulk sediment, pollen concentrate and macrofossil ages revealing lower values compared to previous studies from the lake. A systematic age offset between the pollen and macrofossil indicates that pollen ages are ~340 ^{14}C years older than macrofossil ages. Experimental analysis suggests that the ^{14}C ages of pollen concentrates were affected by the admixture of pollen grains with aquatic algae that incorporated ^{14}C-depleted groundwater during growth. The Bayesian *Plum* model, incorporating corrected pollen and macrofossil ages, ^{210}Pb activity and Pu dates, yielded a final age model for the 11.37 m long composite sediment sequence at Lake Surprise, representing an approximately 10,846 cal yr BP record. This age model explains many of the issues identified in previous studies and its consistency and minimal uncertainties demonstrate the potential of Lake Surprise to form the basis of robust climate interpretations.

CRediT authorship contribution statement

Asika Dharmarathna: Writing – review & editing, Writing – original draft, Visualization, Validation, Software, Methodology, Investigation, Formal analysis, Data curation, Conceptualization. **Haidee Cadd:** Writing – review & editing, Visualization, Validation, Software, Resources, Methodology, Investigation, Formal analysis, Data curation.

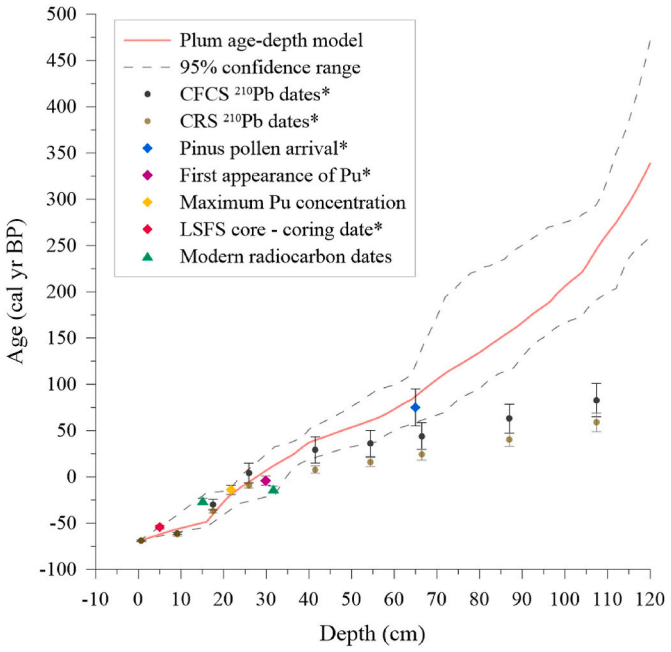

Fig. 8. Representation of recent sediment markers in section top 120 cm of the record. The first appearance of Pu, the coring date of the previous sediment core (LSFS) and *Pinus* pollen arrival were not used in the model. Note that the coring date of the LSFS core and *Pinus* pollen arrival dates were taken from Barr et al. (2014) based on diatom record correlation (Appendix, Fig. A1). Maximum Pu concentration and first appearance of Pu are illustrated as A and B in Fig. 3a. For detailed information refer to (Appendix, Table A6). (* represents the markers that were not incorporated into the age model).

Cameron Barr: Writing – review & editing, Validation, Resources, Methodology, Investigation, Funding acquisition, Formal analysis, Conceptualization. **Alexander Francke:** Writing – review & editing, Visualization, Validation, Software, Investigation, Formal analysis. **Quan Hua:** Writing – review & editing, Resources, Methodology, Investigation, Data curation. **David Child:** Writing – review & editing, Resources, Methodology, Investigation, Data curation. **Michael Hotchkis:** Writing – review & editing, Resources, Methodology, Investigation, Data curation. **Atun Zawadzki:** Writing – review & editing, Resources, Investigation, Formal analysis, Data curation. **Patricia Gadd:** Resources, Investigation, Data curation. **Chris Turney:** Writing – review & editing, Resources, Methodology. **Christopher E. Marjo:** Writing – review & editing, Resources, Methodology. **John Tibby:** Writing – review & editing, Validation, Supervision, Resources, Project administration, Methodology, Funding acquisition, Conceptualization. **Jonathan J. Tyler:** Writing – review & editing, Validation, Supervision, Software, Resources, Project administration, Methodology, Funding acquisition, Conceptualization.

Declaration of competing interest

The authors declare that they have no known competing financial interests or personal relationships that could have appeared to influence the work reported in this paper.

Acknowledgements

This study was mainly supported by an Australian Research Council (ARC) Discovery project (DP190102782). Acquisition of radiocarbon dates, radionuclide dates (210 Pb and Pu isotopes) and ITRAX core scanning were supported by an Australia's Nuclear Science and Technology Organisation (ANSTO) grant (AP12406) awarded to Cameron Barr and by an Australian Institute of Nuclear Science and Engineering

(AINSE) Ltd. Postgraduate Research Award to Asika Dharmarathna (ALNSTU12917). The authors acknowledge the Gunditj Mirring Traditional Owner Aboriginal Corporation and the Parks Victoria team for permission and their assistance in undertaking this work. The Authors would like to thank Bernd Zolitschka, Theodore Cadd, Alan Gontz, and Martin Ankor for their efforts in collecting sediment cores from Lake Surprise. Further, the Authors are grateful to laboratory technicians at the Centre for Accelerator Science, ANSTO, and the Mawson Analytical Spectrometry laboratory, University of Adelaide for their assistance in laboratory sample preparation and analyses.

Appendix. Supplementary data

Section 1: Results of ^{210}Pb and Pu analysis.

Table A1
CFCS and CRS age model calculations

Laboratory code	Mid-point depth (cm)	Dry bulk density (g/cm^3)	Cumulative dry mass (g/cm^2)	Calculated CFCS ages (years)	Mass accumulation (g/cm^2/year)	Calculated CRS ages (years)	Mass accumulation (g/cm^2/year)
W557	0.7	0.03	0.01 ± 0.01	1 ± 1	0.0196 ± 0.003	1 ± 1	0.021 ± 0.001
W558	9.1	0.02	0.15 ± 0.01	8 ± 1		7 ± 2	0.022 ± 0.001
W559	17.5	0.18	0.76 ± 0.03	39 ± 6		32 ± 2	0.029 ± 0.002
W560	25.9	0.04	1.43 ± 0.04	73 ± 11		60 ± 3	0.018 ± 0.002
W561	41.5	0.04	1.92 ± 0.03	98 ± 14		77 ± 4	0.055 ± 0.008
W562	54.3	0.05	2.48 ± 0.03	105 ± 14	0.077 ± 0.016	85 ± 5	0.093 ± 0.015
W563	66.3	0.05	3.11 ± 0.03	113 ± 14		93 ± 6	0.074 ± 0.013
W564	86.9	0.11	4.50 ± 0.03	132 ± 16		109 ± 7	0.098 ± 0.022
W565	107.4	0.07	6.05 ± 0.03	152 ± 18		128 ± 10	0.068 ± 0.020

Table A2
Pu isotope concentrations in the Lake Surprise sediments

Depth range (cm)	Mid-point depth (cm)	Total Pu concentration (pg/g)	$^{241/239}$Pu ratio	$^{240/239}$Pu ratio	$^{239+240}$Pu concentration (mBq/g)
0–1.4	0.7	0.1330 ± 0.0041	4.90E-04 ± 2.13E-04	0.166 ± 0.006	4.20E-01 ± 1.02E-02
4.2–5.6	4.9	0.1832 ± 0.0042	7.32E-04 ± 1.78E-04	0.160 ± 0.004	5.73E-01 ± 1.11E-02
8.4–9.8	9.1	0.3145 ± 0.0068	5.26E-04 ± 9.79E-05	0.130 ± 0.003	9.42E-01 ± 1.68E-02
12.6–14.0	13.3	0.4908 ± 0.0111	7.89E-04 ± 1.29E-04	0.149 ± 0.003	1.51E-00 ± 2.84E-02
16.8–18.2	17.5	1.2416 ± 0.0317	7.81E-04 ± 1.07E-04	0.151 ± 0.003	3.84E-00 ± 8.06E-02
21.0–22.4	21.7	1.3022 ± 0.0268	7.54E-04 ± 1.02E-04	0.168 ± 0.004	4.13E-00 ± 7.27E-02
25.2–26.6	25.9	1.1930 ± 0.0290	8.09E-04 ± 1.19E-04	0.179 ± 0.004	3.84E-00 ± 7.67E-02
29.3–30.6	29.9	0.1073 ± 0.0023	7.79E-04 ± 1.65E-04	0.171 ± 0.005	3.41E-01 ± 6.30E-02
33.2–34.5	33.8	0.0232 ± 0.0007	5.84E-04 ± 3.29E-04	0.168 ± 0.007	7.36E-02 ± 1.79E-02
37.1–38.4	37.7	0.0486 ± 0.0011	1.33E-04 ± 7.85E-05	0.079 ± 0.002	1.33E-01 ± 1.33E-02

Section 2: Age-depth modelling.
Prior information was used to develop the age model for the Lake Surprise sediments are as follows.

Table A3
The radiocarbon ages (corrected for the age offset based on the ^{14}C age difference between pollen and macrofossil at 136.45 cm depth) and recent sediment dates (core surface, and Pu Peak) used in the age model of the Lake Surprise sediment (These data were saved as "**LakeSurprise6_C**" in a CSV file).

Material dated	Depth (cm)	Lab ID	^{14}C age		Delta.R	Delta.STD
			Mean	1σ		
Core surface	0	–	−69	3	0	0
Plant	15.05	OZZ426	−13	3	0	0
Pu peak	21.7	–	−14	3	0	0
Plant	31.55	OZZ427	−22	3	0	0
Pollen	41.2	UNSW-490	314	20	340	50
Pollen	52.15	UNSW-491	375	20	340	50
Pollen	62.15	UNSW-492	387	20	340	50
Plant	69.15	OZZ428	520	20	0	0
Pollen	73.45	UNSW-493	423	20	340	50
Pollen	77.65	UNSW-497	451	20	340	50
Macrofossil	96.2	OZZ429	255	20	0	0
Pollen	97.3	UNSW-494	475	20	340	50
Pollen	104.45	UNSW-526	565	20	340	50
Pollen	116.65	UNSW-495	581	20	340	50
Macrofossil	129.3	OZZ514	460	22	0	0
Macrofossil	**136.45**	**OZZ430**	**525**	**20**	**0**	**0**
Pollen	**136.45**	**UNSW-496**	**865**	**20**	**340**	**50**
Pollen	151.51	UNSW-499	939	20	340	50
Pollen	188	UNSW-500	1666	20	340	50

(*continued on next page*)

Table A3 (*continued*)

Material dated	Depth (cm)	Lab ID	^{14}C age		Delta.R	Delta.STD
			Mean	1σ		
Plant	214	OZZ516	1262	18	0	0
Pollen	218	UNSW-501	1549	20	340	50
Pollen	253	UNSW-502	1760	20	340	50
Pollen	274.5	UNSW-503	2026	20	340	50
Plant	288	OZZ518	1858	22	0	0
Pollen	310.5	UNSW-504	2424	20	340	50
Pollen	348.5	UNSW-505	2537	20	340	50
Macrofossil	375.5	OZZ521	2331	21	0	0
Plant	379.5	OZZ520	2235	24	0	0
Pollen	407.5	UNSW-506	2862	20	340	50
Pollen	450	UNSW-507	3291	20	340	50
Pollen	479	UNSW-530	3329	20	340	50
Plant	497	OZZ522	3091	21	0	0
Pollen	509.5	UNSW-510	3442	20	340	50
Pollen	541.5	UNSW-511	3525	20	340	50
Plant	566	OZZ524	3866	20	0	0
Pollen	579	UNSW-512	3976	20	340	50
Pollen	608.5	UNSW-531	3984	20	340	50
Pollen	717.5	UNSW-516	4785	20	340	50
Plant	744.5	OZZ525	4775	23	0	0
Plant	776.5	OZZ526	5029	24	0	0
Macrofossil	782.5	OZZ527	5124	23	0	0
Pollen	809	UNSW-517	5682	20	340	50
Pollen	854.5	UNSW-518	6625	20	340	50
Plant	898	OZZ528	6297	25	0	0
Pollen	924	UNSW-519	6847	20	340	50
Pollen	956	UNSW-520	7428	20	340	50
Pollen	982	UNSW-521	7408	20	340	50
Pollen	1016	UNSW-522	8049	20	340	50
Pollen	1056.5	UNSW-523	8658	20	340	50
Pollen	1132.5	UNSW-524	10034	20	340	50

Table A4
The ^{210}Pb activity data used in the age model of the Lake Surprise sediment (These data were saved as "**LakeSurprise6**" in a CSV file).

Lab ID	depth (cm)	Density (g/cm)	^{210}Pb activity (Bq/kg)	Standard deviation (^{210}Pb)	Thickness (cm)
W557	0.7	0.03	906	47	0.7
W558	9.1	0.02	719	35	0.7
W559	17.5	0.18	253	11	0.7
W560	25.9	0.04	170	8	0.7
W561	41.5	0.04	35	2	0.7
W562	54.3	0.05	18	1	0.7
W563	66.3	0.05	17	1	0.7
W564	86.9	0.11	9	1	0.7
W565	107.4	0.07	9	1	0.7

Table A5
Modern age markers used in Fig. 8 (for CFCS/CRS data see Table A1)

Sample	Depth (cm)	Age (CE)	Age (cal yr BP)	Age error
Pinus (LSFS core)	65.0	1875	75.0	20
modern C	15.1	1976	−26.0	3
modern C	31.6	1963	−13.0	3
Pu peak	21.7	1964	−14.0	5
Pu appearance	29.9	1954	−4.0	–
LSFS coring age	5.0	2004	−54.0	2

Section 3: FTIR analysis.

Table A6
Radiocarbon-dated pollen samples analysed for the FTIR spectrum

Sample ID	Composite depth (cm) of the sample	Age-offset (pollen-macrofossil) cal yr BP
UNSW-494	97.3	49.1
UNSW-495	116.65	187
UNSW-496	136.45	213

(*continued on next page*)

Table A6 (*continued*)

Sample ID	Composite depth (cm) of the sample	Age-offset (pollen-macrofossil) cal yr BP
UNSW-500	188	456
UNSW-501	218	339
UNSW-502	253	386
UNSW-503	274.5	407
UNSW-504	310.5	522

FTIR sample analysis: For each sample, approximately 1–2 mg of powdered pollen material was placed on the ATR crystal, and sufficient pressure was applied to ensure full contact with the crystal. Spectral data were collected in transmission mode, at a resolution of 4 cm^{-1} over a spectral range of 4000–400 cm^{-1} (2.5–25 μm). The analysis was performed in a temperature-controlled laboratory at room temperature (25 °C). Background spectra were collected prior to analysis of each sample and automatically subtracted from the spectral data to minimise the interference between the crystal and the sample.

Table A7: Summary of ITRAX data (Ca (%)) and age-depth model data showing the age differences between pollen and macrofossil samples across sediment depth, as used in Fig. 5 (Data will be uploaded to the NOAA & PANGEA repositories upon acceptance).

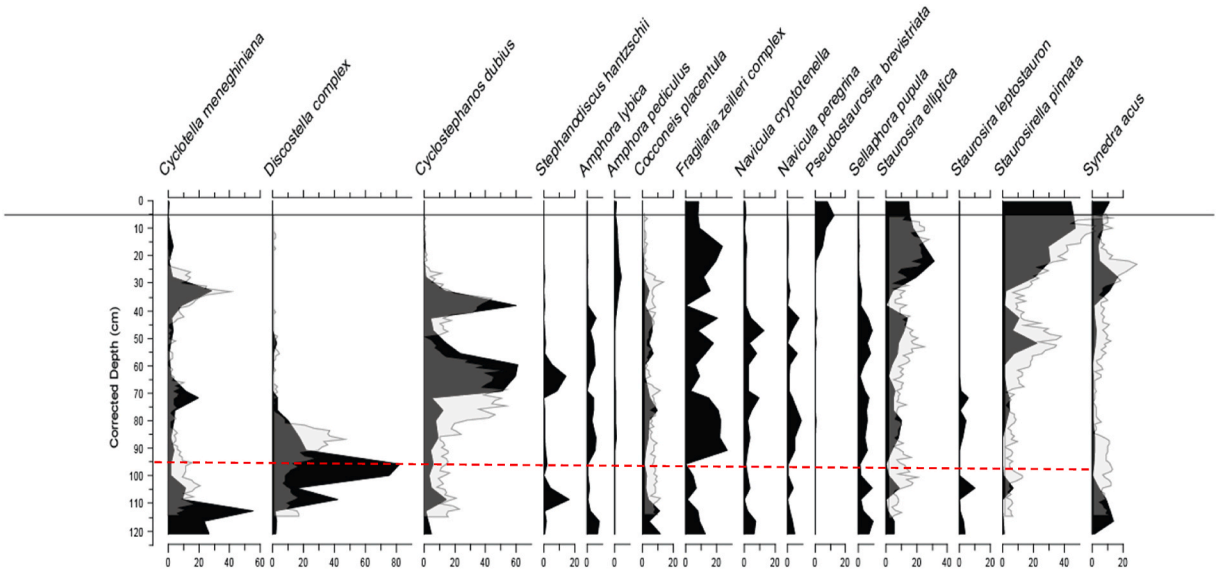

Fig. A1. Comparison of diatom data from SUR-19-01 (Black-shaded) and the LSFS sediment core recovered in 2004 (Barr et al., 2014) (grey-shaded). Only the most common taxa are shown here. The top of LSFS, indicated by the black horizontal line, corresponds to a depth of 5 cm in SUR-19-01. This gives this depth an age of 15 years from the SUR-19-1 2019 coring date and a sedimentation rate of 5 yr cm^{-1}, which is consistent with the age-depth relationship derived from other means. Also, the depth of the first appearance of *Pinus* pollen in the LSFS core is shown by the red dotted line (90 cm)

Fig. A2. Stratigraphic representation of core images from Lake Surprise sediments (cores SUR-19-02 and SUR-19-03). Both cores were retrieved in 1 m drive sections, with the surface of the SUR-19-03 core approximately 0.5 m below that of SUR-19-02. The zoomed-in section (SUR-19-02; 6–7 m) highlights well-preserved, undisturbed fine laminations observed throughout the sediment profile. This interval was selected to illustrate the undisturbed fine lamination structure, despite the presence of age reversals observed in samples from this depth (Core stratigraphy was developed by Cameron Barr).

Data availability

The data that support Fig. 5 of this study will be uploaded to the NOAA and PANGEA repositories upon acceptance. Supplementary data supporting the findings of this study are available in the Appendix section.

References

Abdala Díaz, R.T., Casas Arrojo, V., Arrojo Agudo, M.A., Cárdenas, C., Dobretsov, S., Figueroa, F.L., 2019. Immunomodulatory and antioxidant activities of sulfated polysaccharides from laminaria ochroleuca, porphyra umbilicalis, and gelidium corneum. Mar. Biotechnol. 21 (4), 577–587. https://doi.org/10.1007/s10126-019-09905-x.

Abril, J.M., 2019. Radiometric dating of recent sediments: on the performance of 210Pb-based CRS chronologies under varying rates of supply. Quat. Geochronol. 51, 1–14. https://doi.org/10.1016/j.quageo.2018.12.003.

Ankor, M.J., Tyler, J.J., 2022. A computational method for rapid orthographic photography of lake sediment cores. J. Paleolimnol., 0123456789 https://doi.org/10.1007/s10933-022-00241-0.
Appleby, P.G., 1998. Dating Recent Sediments by 210 Pb: Problems and Solutions, pp. 7–24. No. STUK-A–145.
Appleby, P.G., 2001. Chronostratigraphic techniques in recent sediments. Tracking environmental change using lake sediments: basin analysis, coring, and chronological techniques 171–203. https://doi.org/10.1007/0-306-47669-X_9.
Appleby, P.G., 2008. Three decades of dating recent sediments by fallout radionuclides: a review. Holocene 18 (1), 83–93. https://doi.org/10.1177/0959683607085598.
Appleby, P.G., Oldfield, F., 1978. The calculation of lead-210 dates assuming a constant rate of supply of unsupported 210Pb to the sediment. Catena (Cremling.) 5 (1), 1–8. https://doi.org/10.1016/S0341-8162(78)80002-2.
Appleby, P.G., Oldfield, F., Thompson, R., Huttunen, P., Tolonen, K., 1979. 210Pb dating of annually laminated lake sediments from Finland [10]. Nature 280 (5717), 53–55. https://doi.org/10.1038/280053a0.
Australian Bureau of Meteorology, 2021. Annual report 2020–21. available online: https://www.bom.gov.au/inside/Annual_Report/2020-21/. (Accessed 30 May 2022).
Aquino-López, M.A., Blaauw, M., Christen, J.A., Sanderson, N.K., 2018. Bayesian analysis of 210 Pb dating. J. Agric. Biol. Environ. Stat. 23 (3), 317–333. https://doi.org/10.1007/s13253-018-0328-7.
Aquino-López, M.A., Ruiz-Fernández, A.C., Blaauw, M., Sanchez-Cabeza, J.A., 2020a. Comparing classical and Bayesian 210Pb dating models in human-impacted aquatic environments. Quat. Geochronol. 60. https://doi.org/10.1016/j.quageo.2020.101106.
Aquino-López, M.A., Sanderson, N.K., Blaauw, M., Sanchez-Cabeza, J.-A., Ruiz-Fernandez, A.C., Aquino-López, J.A.C.M.A., Sanderson, N.K., Blaauw, M., Sanchez-Cabeza, J.-A., Ruiz-Fernandez, A.C., Christen, J.A., 2020b. A simulation study to compare 210Pb dating data analyses, 1–21. http://arxiv.org/abs/2012.06819.
Barr, C., Tibby, J., Gell, P., Tyler, J., Zawadzki, A., Jacobsen, G.E., 2014. Climate variability in south-eastern Australia over the last 1500 years inferred from the high-resolution diatom records of two crater lakes. Quat. Sci. Rev. 95, 115–131. https://doi.org/10.1016/j.quascirev.2014.05.001.
Barsanti, M., Garcia-Tenorio, R., Schirone, A., Rozmaric, M., Ruiz-Fernández, A.C., Sanchez-Cabeza, J.A., Delbono, I., Conte, F., De Oliveira Godoy, J.M., Heijnis, H., Eriksson, M., Hatje, V., Laissaoui, A., Nguyen, H.Q., Okuku, E., Al-Rousan, S.A., Uddin, S., Yii, M.W., Osvath, I., 2020. Challenges and limitations of the 210Pb sediment dating method: results from an IAEA modelling interlaboratory comparison exercise. Quat. Geochronol. 59. https://doi.org/10.1016/j.quageo.2020.101093.
Baskaran, M., Nix, J., Kuyper, C., Karunakara, N., 2014. Problems with the dating of sediment core using excess 210Pb in a freshwater system impacted by large scale watershed changes. J. Environ. Radioact. 138, 355–363. https://doi.org/10.1016/j.jenvrad.2014.07.006.
Battarbee, R.W., Jones, V.J., Flower, R.J., Cameron, N.G., Bennion, H., Carvalho, L., Juggins, S., 2001. Diatoms. In: Smol, J.P., Birks, H.J.B., Last, W.M. (Eds.), Tracking Environmental Change Using Lake Sediments: Volume 3: Terrestrial, Algal, and Siliceous Indicators. Springer, pp. 155–202.
Benoit, G., Rozan, T.F., 2001. 210Pb and 137Cs dating methods in lakes: a retrospective study. J. Paleolimnol. 25 (4), 455–465. https://doi.org/10.1023/A:1011179318352.
Björck, S., Wohlfarth, B., 2001. 14 C chronostratigraphic techniques in paleolimnology. Tracking Environmental Change Using Lake Sediments: Basin Analysis, Coring, and Chronological Techniques. Springer, pp. 205–245. https://doi.org/10.1007/0-306-47669-X_10.
Blaauw, M., Christen, J.A., 2011. Flexible paleoclimate age-depth models using an autoregressive gamma process. Bayesian Analysis 6 (3), 457–474. https://doi.org/10.1214/11-BA618.
Blaauw, M., Christen, J.A., Aquino-López, M.A., 2020. A review of statistics in palaeoenvironmental research. J. Agric. Biol. Environ. Stat. 25 (1), 17–31. https://doi.org/10.1007/s13253-019-00374-2.
Brenner, M., Kenney, W.F., 2015. Dating wetland sediment cores. Methods in Biogeochemistry of Wetlands 10, 879–900. https://doi.org/10.2136/sssabookser10.c45.
Builth, H., Kershaw, A.P., White, C., Roach, A., Hartney, L., McKenzie, M., Lewis, T., Jacobsen, G., 2008. Environmental and cultural change on the Mt Eccles lava-flow landscapes of southwest Victoria, Australia. Holocene 18 (3), 413–424. https://doi.org/10.1177/0959683607087931.
Cadd, H., Sherborne-Higgins, B., Becerra-Valdivia, L., Tibby, J., Barr, C., Forbes, M., Cohen, T.J., Tyler, J., Vandergoes, M., Francke, A., Lewis, R., Arnold, L.J., Jacobsen, G., Marjo, C., Turney, C., 2022. The application of pollen radiocarbon dating and bayesian age-depth modeling for developing robust geochronological frameworks of wetland archives. Radiocarbon 64 (2), 213–235. https://doi.org/10.1017/RDC.2022.29.
Cartwright, I., Currell, M.J., Cendón, D.I., Meredith, K.T., 2020. A review of the use of radiocarbon to estimate groundwater residence times in semi-arid and arid areas. J. Hydrol. 580 (July 2019), 124247. https://doi.org/10.1016/j.jhydrol.2019.124247.
Chen, Y., Zou, C., Mastalerz, M., Hu, S., Gasaway, C., Tao, X., 2015. Applications of micro-fourier transform infrared spectroscopy (FTIR) in the geological sciences—a Review. Int. J. Mol. Sci. 16 (12), 30223–30250. https://doi.org/10.3390/ijms161226227.
Child, D.P., Hotchkis, M.A.C., 2013. Nuclear Instruments and Methods in Physics Research B Plutonium and uranium contamination in soils from former nuclear weapon test sites in Australia. Nuclear Inst. and Methods in Physics Research 642–646. https://doi.org/10.1016/j.nimb.2012.05.018. B, 294.
Child, D.P., Hotchkis, M.A.C., Williams, M.L., 2008. High sensitivity analysis of plutonium isotopes in environmental samples using accelerator mass spectrometry (AMS). Journal of Analytical Atomic Spectrometry 23 (5), 765–768. https://doi.org/10.1039/b715788f.
Corcho-Alvarado, J.A., Diaz-Asencio, M., Froidevaux, P., Bochud, F., Alonso-Hernández, C.M., Sanchez-Cabeza, J.A., 2014. Dating young Holocene coastal sediments in tropical regions: use of fallout 239,240Pu as alternative chronostratigraphic marker. Quat. Geochronol. 22, 1–10. https://doi.org/10.1016/j.quageo.2014.02.001.
Croudace, I.W., Rindby, A., Rothwell, R.G., 2006. ITRAX: Description and Evaluation of a New Multi-Function X-Ray Core Scanner, vol. 267. Geological Society Special Publication, pp. 51–63. https://doi.org/10.1144/GSL.SP.2006.267.01.04.
Dharmarathna, B.P.G.A.M.K., 2022. Holocene Hydroclimate Variability in South-Eastern Australia: Validation and Application of Cellulose Oxygen Isotopes at Lake Surprise. University of Adelaide Digital Library, Victoria, Australia *[Doctoral dissertation, University of Adelaide]*. https://hdl.handle.net/2440/138507.
De Deckker, P., 2022. The Holocene hypsithermal in the Australian region. Quaternary Science Advances 7 (8), 100061. https://doi.org/10.1016/j.qsa.2022.100061.
Dingemans, T., Mensing, S.A., Feakins, S.J., Kirby, M.E., Zimmerman, S.R.H., 2014. 3000 years of environmental change at Zaca Lake, California, USA. Frontiers in Ecology and Evolution 2 (7), 1–16. https://doi.org/10.3389/fevo.2014.00034.
El-Eswed, B., 2016. Effect of basicity and hydrophobicity of amines on their adsorption onto charcoal. Desalination Water Treat. 57 (41), 19227–19238. https://doi.org/10.1080/19443994.2015.1101622.
Everett, S.E., Tims, S.G., Hancock, G.J., Bartley, R., Fifield, L.K., 2008. Comparison of Pu and ^{137}Cs as tracers of soil and sediment transport in a terrestrial environment. J. Environ. Radioact. 99 (2), 383–393. https://doi.org/10.1016/j.jenvrad.2007.07.007.
Falster, G., Tyler, J., Grant, K., Tibby, J., Turney, C., Löhr, S., Jacobsen, G., Kershaw, A. P., 2018. Millennial-scale variability in south-east Australian hydroclimate between 30,000 and 10,000 years ago. Quat. Sci. Rev. 192, 106–122. https://doi.org/10.1016/j.quascirev.2018.05.031.
Fink, D., Hotchkis, M., Hua, Q., Jacobsen, G., Smith, A.M., Zoppi, U., Child, D., Mifsud, C., Van Der Gaast, H., Williams, A., Williams, M., 2004. The ANTARES AMS facility at ANSTO. Nucl. Instrum. Methods Phys. Res., Sect. B: Beam Interactions with Materials and Atoms, 223–224(SPEC. ISS.) 109–115. https://doi.org/10.1016/j.nimb.2004.04.025.
Fletcher, M.S., Thomas, I., 2010. A quantitative Late Quaternary temperature reconstruction from western Tasmania, Australia. Quat. Sci. Rev. 29 (17–18), 2351–2361. https://doi.org/10.1016/j.quascirev.2010.06.012.
Fletcher, W.J., Zielhofer, C., Mischke, S., Bryant, C., Xu, X., Fink, D., 2017. AMS radiocarbon dating of pollen concentrates in a karstic lake system. Quat. Geochronol. 39, 112–123. https://doi.org/10.1016/j.quageo.2017.02.006.
Forbes, M., Cohen, T., Jacobs, Z., Marx, S., Barber, E., Dodson, J., Zamora, A., Cadd, H., Francke, A., Constantine, M., Mooney, S., Short, J., Tibby, J., Parker, A., Cendón, D., Peterson, M., Tyler, J., Swallow, E., Haines, H., Woodward, C., 2021. Comparing interglacials in eastern Australia: a multi-proxy investigation of a new sedimentary record. Quat. Sci. Rev. 252. https://doi.org/10.1016/j.quascirev.2020.106750.
Gell, P., Tibby, J., Fluin, J., Leahy, P., Reid, M., Adamson, K., Bulpin, S., MacGregor, A., Wallbrink, P., Hancock, G., Walsh, B., 2005. Accessing limnological change and variability using fossil diatom assemblages, south-east Australia. River Res. Appl. 21 (2–3), 257–269. https://doi.org/10.1002/rra.845.
Goldberg, E.D., 1963. Geochronology with Pb-210, Radioactive Dating. International Atomic Energy Agency.
Gouramanis, C., De Deckker, P., Switzer, A.D., Wilkins, D., 2013. Cross-continent comparison of high-resolution Holocene climate records from southern Australia: deciphering the impacts of far-field teleconnections. Earth Sci. Rev. 121, 55–72. https://doi.org/10.1016/j.earscirev.2013.02.006.
Graham, K.J., Daley, R.K., 2011. Distribution, reproduction and population structure of three gulper sharks (Centrophorus, Centrophoridae) in south-east Australian waters. Mar. Freshw. Res. 62 (6), 583–595. https://doi.org/10.1071/MF10158.
Hancock, G.J., Leslie, C., Everett, S.E., Tims, S.G., Brunskill, G.J., Haese, R., 2011. Plutonium as a chronomarker in Australian and New Zealand sediments: a comparison with 137Cs. J. Environ. Radioact. 102 (10), 919–929. https://doi.org/10.1016/j.jenvrad.2009.09.008.
Hancock, G.J., Tims, S.G., Fifield, L.K., Webster, I.T., 2014. The release and persistence of radioactive anthropogenic nuclides. Geological Society Special Publication 395 (1), 265–281. https://doi.org/10.1144/SP395.15.
Harle, K.J., Etheridge, D.M., Whetton, P., Jones, R., Hennessy, K., Goodwin, I.D., Nicholls, N., 2005. Building a future on knowledge from the past: what palaeo-science can reveal about climate change and its potential impacts in Australia, vol. 1. Australian Greenhouse Office, pp. 1–46.
Harris, S., Mills, G., Brown, T., 2017. Variability and drivers of extreme fire weather in fire-prone areas of south-eastern Australia. Int. J. Wildland Fire 26 (3), 177–190. https://doi.org/10.1071/WF16118.
Harrison, J., Heijnis, H., Caprarelli, G., 2003. Historical pollution variability from abandoned mine sites, greater blue mountains World heritage area, New South wales, Australia. Environ. Geol. 43 (6), 680–687. https://doi.org/10.1007/s00254-002-0687-8.
Harrison, J.J., Saunders, K.M., Child, D.P., Hotchkis, M.A.C., 2021. A record of fallout 239Pu and 240Pu at World heritage bathurst harbour, Tasmania, Australia. J. Environ. Radioact. 237. https://doi.org/10.1016/j.jenvrad.2021.106679.
Heijnis, H., 2001. The Principle of 210Pb Dating of Sediments. Archives of Human Impact. Australian Institute of Nuclear Science and Engineering, Sydney, pp. 3–13. Retrieved from. https://www.researchgate.net/publication/266376025.
Hirose, K., Aoyama, M., 2003. Present background levels of surface 137Cs and 239,240Pu concentrations in the Pacific. J. Environ. Radioact. 69 (1–2), 53–60. https://doi.org/10.1016/S0265-931X(03)00086-9.

Hirose, K., Povinec, P.P., 2015. Sources of plutonium in the atmosphere and stratosphere-troposphere mixing. Sci. Rep. 5, 1–9. https://doi.org/10.1038/srep15707.
Hogg, A.G., Heaton, T.J., Hua, Q., Palmer, J.G., Turney, C.S.M., Southon, J., Bayliss, A., Blackwell, P.G., Boswijk, G., Bronk Ramsey, C., Pearson, C., Petchey, F., Reimer, P., Reimer, R., Wacker, L., 2020. SHCal20 southern Hemisphere calibration, 0-55,000 Years cal BP. Radiocarbon 62 (4), 759–778. https://doi.org/10.1017/RDC.2020.59.
Hollins, S.E., Harrison, J.J., Jones, B.G., Zawadzki, A., Heijnis, H., Hankin, S., 2011. Reconstructing recent sedimentation in two urbanised coastal lagoons (NSW, Australia) using radioisotopes and geochemistry. J. Paleolimnol. 46 (4), 579–596. https://doi.org/10.1007/s10933-011-9555-4.
Holmgren, S.U., Bigler, C., Ingólfsson, Ó., Wolfe, A.P., 2010. The Holocene-Anthropocene transition in lakes of western spitsbergen, Svalbard (Norwegian high arctic): climate change and nitrogen deposition. J. Paleolimnol. 43 (2), 393–412. https://doi.org/10.1007/s10933-009-9338-3.
Hong, T., Yin, J.Y., Nie, S.P., Xie, M.Y., 2021. Applications of infrared spectroscopy in polysaccharide structural analysis: progress, challenge and perspective. Food Chem. X 12 (November), 100168. https://doi.org/10.1016/j.fochx.2021.100168.
Hotchkis, M.A.C., Child, D.P., Froehlich, M.B., Wallner, A., Wilcken, K., Williams, M., 2019. Actinides AMS on the VEGA accelerator. Nuclear Instruments and Methods in Physics Research, Section B: Beam Interactions with Materials and Atoms 438, 70–76. https://doi.org/10.1016/j.nimb.2018.07.029. January 2018.
Howarth, J.D., Fitzsimons, S.J., Jacobsen, G.E., Vandergoes, M.J., Norris, R.J., 2013. Identifying a reliable target fraction for radiocarbon dating sedimentary records from lakes. Quat. Geochronol. 17, 68–80. https://doi.org/10.1016/j.quageo.2013.02.001.
Hua, Q., Barbetti, M., Levchenko, V.A., D'Arrigo, R.D., Buckley, B.M., Smith, A.M., 2012. Monsoonal influence on southern Hemisphere 14CO2. Geophys. Res. Lett. 39 (19), 1–5. https://doi.org/10.1029/2012GL052971.
Hua, Q., Barbetti, M., Rakowski, A.Z., 2013. Atmospheric radiocarbon for the period 1950–2010. Radiocarbon 55 (4), 2059–2072. https://doi.org/10.2458/azu_js_rc.v55i2.16177.
Hua, Q., Jacobsen, G.E., Zoppi, U., Lawson, E.M., Williams, A.A., Smith, A.M., McGann, M.J., 2001. Progress in radiocarbon target preparation at the ANTARES AMS centre. Radiocarbon 43 (2 PART I), 275–282. https://doi.org/10.1017/s003382220003811x.
Hua, Q., Turnbull, J.C., Santos, G.M., Rakowski, A.Z., Ancapichún, S., De Pol-Holz, R., Hammer, S., Lehman, S.J., Levin, I., Miller, J.B., Palmer, J.G., Turney, C.S.M., 2022. Atmospheric radiocarbon for the period 1950-2019. Radiocarbon 64 (4), 723–745. https://doi.org/10.1017/RDC.2021.95.
Jakopi, R., Richter, S., Kühn, H., Aregbe, Y., 2010. Determination of 240Pu/239Pu, 241Pu/239Pu and 242Pu/239Pu isotope ratios in environmental reference materials and samples from Chernobyl by thermal ionization mass spectrometry (TIMS) and filament carburization. Journal of Analytical Atomic Spectrometry 25 (6), 815–821. https://doi.org/10.1039/b925918j.
Jebsen, C., Norici, A., Wagner, H., Palmucci, M., Giordano, M., Wilhelm, C., 2012. FTIR spectra of algal species can be used as physiological fingerprints to assess their actual growth potential. Physiol. Plantarum 146 (4), 427–438. https://doi.org/10.1111/j.1399-3054.2012.01636.x.
Johansen, M.P., Child, D.P., Caffrey, E.A., Davis, E., Harrison, J.J., Hotchkis, M.A.C., Payne, T.E., Ikeda-ohno, A., Thiruvoth, S., Twining, J.R., Beresford, N.A., 2016. Accumulation of plutonium in mammalian wildlife tissues following dispersal by accidental-release tests. J. Environ. Radioact. 151, 387–394. https://doi.org/10.1016/j.jenvrad.2015.03.031.
Johansen, M.P., Child, D.P., Cresswell, T., Harrison, J.J., Hotchkis, M.A.C., Howell, N.R., Johansen, A., Sdraulig, S., Thiruvoth, S., Young, E., Whiting, S.D., 2019. Science of the Total Environment Plutonium and other radionuclides persist across marine-to-terrestrial ecotopes in the Montebello Islands sixty years after nuclear tests. Sci. Total Environ. 691, 572–583. https://doi.org/10.1016/j.scitotenv.2019.06.531.
Kelley, J.M., Bond, L.A., Beasley, T.M., 1999. Global distribution of Pu isotopes and 237Np. Sci. Total Environ. 237–238, 483–500. https://doi.org/10.1016/S0048-9697(99)00160-6.
Kershaw, A.P., Clark, J.S., Gill, A.M., D'Costa, D.M., 2002. A history of fire in Australia. Flammable Australia: the Fire Regimes and Biodiversity of a Continent. Cambridge University Press, pp. 3–25.
Kiem, A.S., Johnson, F., Westra, S., van Dijk, A., Evans, J.P., O'Donnell, A., Rouillard, A., Barr, C., Tyler, J., Thyer, M., Jakob, D., Woldemeskel, F., Sivakumar, B., Mehrotra, R., 2016. Natural hazards in Australia: droughts. Clim. Change 139 (1), 37–54. https://doi.org/10.1007/s10584-016-1798-7.
Kilian, M.R., Van Der Plicht, J., Van Geel, B., Goslar, T., 2002. Problematic 14C-AMS dates of pollen concentrates from Lake Gosciaz (Poland). Quat. Int. 88 (1), 21–26. https://doi.org/10.1016/S1040-6182(01)00070-2.
Kirchner, G., 2011. 210Pb as a tool for establishing sediment chronologies: examples of potentials and limitations of conventional dating models. J. Environ. Radioact. 102 (5), 490–494. https://doi.org/10.1016/j.jenvrad.2010.11.010.
Koide, M., Michel, R., Goldberg, E.D., Herron, M.M., Langway Jr., C.C., 1982. Characterization of radioactive fallout from pre- and post-moratorium tests to polar ice caps. Nature 296 (5857), 544–547. https://doi.org/10.1038/296544a0.
Korsman, T., Renberg, I., Dåbakk, E., Nilsson, M.B., 2005. Near-infrared spectrometry (nirs) in palaeolimnology. Tracking Environmental Change Using Lake Sediments 2, 299–317. https://doi.org/10.1007/0-306-47670-3_11.
Kosnik, M.A., Hua, Q., Kaufman, D.S., Zawadzki, A., 2015. Sediment accumulation, stratigraphic order, and the extent of time-averaging in lagoonal sediments: a comparison of 210Pb and 14C/amino acid racemization chronologies. Coral Reefs 34 (1), 215–229. https://doi.org/10.1007/s00338-014-1234-2.
Kotov, S., Pälike, H., 2018. QAnalySeries-a cross-platform time series tuning and analysis tool. AGU Fall Meeting Abstracts. Vol. 2018, pp. PP53D-1230.
Kovac, N., Faganeli, J., Bajt, O., Orel, B., Surca Vuk, A., 2005. Investigation of sediment samples from the Gulf of Trieste (northern Adriatic) by FTIR spectroscopy. Materials and Geoenvironment 52 (1), 81.
Krey, P.W., Hardy, E.P., Pachucki, C., Rourke, F., Coluzza, J., Benson, W.K., 1976. Mass isotopic composition of global fall-out plutonium in soil. In: In Transuranium Nuclides in the Environment. International Atomic Energy Agency, pp. 671–678.
Krishnaswamy, S., Lal, D., Martin, J.M., Meybeck, M., 1971. Geochronology of lake sediments. Earth Planet Sci. Lett. 11 (1–5), 407–414.
Kron, P., Loureiro, J., Castro, S., Čertner, M., 2021. Flow cytometric analysis of pollen and spores: an overview of applications and methodology. Cytometry A 99 (4), 348–358. https://doi.org/10.1002/cyto.a.24330.
Leslie, C., Hancock, G.J., 2008. Estimating the date corresponding to the horizon of the first detection of 137Cs and 239+240Pu in sediment cores. J. Environ. Radioact. 99 (3), 483–490. https://doi.org/10.1016/j.jenvrad.2007.08.016.
Liu, X., Colman, S.M., Brown, E.T., Minor, E.C., Li, H., 2013. Estimation of carbonate, total organic carbon, and biogenic silica content by FTIR and XRF techniques in lacustrine sediments. J. Paleolimnol. 50 (3), 387–398. https://doi.org/10.1007/s10933-013-9733-7.
Long, A., Davis, O.K., De Lanois, J., 1992. Separation and 14C dating of pure pollen from lake sediments: nanofossil AMS dating. Radiocarbon 34 (3), 557–560. https://doi.org/10.1017/S0033822200063827.
Lowe, J.J., 1982. Three flandrian pollen profiles from the teith valley, Perthshire, Scotland: II. Analysis of deteriorated pollen. New Phytol. 90 (2), 371–385. https://doi.org/10.1111/j.1469-8137.1982.tb03268.x.
Mariani, M., Connor, S.E., Theuerkauf, M., Herbert, A., Kuneš, P., Bowman, D., Fletcher, M.-S., Head, L., Kershaw, A.P., Haberle, S.G., Stevenson, J., Adeleye, M., 2022. Disruption of cultural burning promotes shrub encroachment and unprecedented wildfires 292–300. https://doi.org/10.1002/fee.2395.
Martin, L., Goff, J., Jacobsen, G., Mooney, S., 2019. The radiocarbon ages of different organic components in the mires of Eastern Australia. Radiocarbon 61 (1), 173–184. https://doi.org/10.1017/RDC.2018.118.
Marty, J., Myrbo, A., 2014. Radiocarbon dating suitability of aquatic plant macrofossils. J. Paleolimnol. 52 (4), 435–443. https://doi.org/10.1007/s10933-014-9796-0.
Matchan, E.L., Phillips, D., Jourdan, F., Oostingh, K., 2020. Early human occupation of southeastern Australia: newinsights from 40Ar/39Ar dating of young volcanoes. Geology 48 (4), 390–394. https://doi.org/10.1130/G47166.1.
Maxson, C., Tibby, J., Marshall, J., Kent, M., Tyler, J., Barr, C., McGregor, G., Cadd, H., Schulz, C., Lomax, B.H., 2021. Fourier transform infrared spectroscopy as a tracer of organic matter sources in lake sediments. Palaeogeogr. Palaeoclimatol. Palaeoecol. 581 (August), 110622. https://doi.org/10.1016/j.palaeo.2021.110622.
Mazumder, D., Saintilan, N., Hollins, S., Meredith, K., Jacobsen, G., Kobayashi, T., Wen, L., 2019. Carbon uptake in surface water food webs fed by palaeogroundwater. J. Geophys. Res.: Biogeosciences 124 (5), 1171–1180. https://doi.org/10.1029/2018JG004925.
Mecozzi, M., Pietrantonio, E., Amici, M., Romanelli, G., 2001. Determination of carbonate in marine solid samples by FTIR-ATR spectroscopy. Analyst 126 (2), 144–146. https://doi.org/10.1039/b009031j.
Mecozzi, M., Pietrantonio, E., Pietroletti, M., 2009. The roles of carbohydrates, proteins and lipids in the process of aggregation of natural marine organic matter investigated by means of 2D correlation spectroscopy applied to infrared spectra. Spectrochimica Acta - Part A: Molecular and Biomolecular Spectroscopy 71 (5), 1877–1884. https://doi.org/10.1016/j.saa.2008.07.015.
Meng, B., Zhou, A., Zhang, Y., Song, M., Liu, W., Xie, Z., Li, S., Liu, Z., 2020. Downcore variations of carbon reservoir ages linked to lake level changes in northwest China. Quat. Geochronol. 55. https://doi.org/10.1016/j.quageo.2020.101105. *Article 101105*.
Mensing, S.A., Southon, J.R., 1999. A simple method to separate pollen for AMS radiocarbon dating and its application to lacustrine and marine sediments. Radiocarbon 41 (1), 1–8. https://doi.org/10.1017/S0033822200019287.
Muramatsu, Y., Uchida, S., Tagami, K., Yoshida, S., Hamilton, T., Robison, W., 2001. Measurement of $^{240}Pu/^{239}Pu$ isotopic ratios in soils from the Marshall Islands using ICP-MS. Sci. Total Environ. 278 (1–3), 151–159. https://doi.org/10.1016/S0048-9697(01)00644-1.
Neulieb, T., Levac, E., Southon, J., Lewis, M., Pendea, I.F., Chmura, G.L., 2013. Potential pitfalls of pollen dating. Radiocarbon 55 (3), 1142–1155. https://doi.org/10.1017/s0033822200048050.
Ninnes, S., Meyer-Jacob, C., Tolu, J., Bindler, R., Cortizas, A.M., 2024. Application of mid-infrared spectroscopy for the quantitative and qualitative analysis of organic matter in Holocene sediment records. Holocene 34 (3), 259–273. https://doi.org/10.1177/09596836231211872.
Nittrouer, C.A., Sternberg, R.W., Carpenter, R., Bennett, J.T., 1979. The use of Pb-210 geochronology as a sedimentological tool: application to the Washington continental shelf. Mar. Geol. 31 (3–4), 297–316. https://doi.org/10.1016/0025-3227(79)90039-2.
Norris, M.W., Turnbull, J.C., Howarth, J.D., Vandergoes, M.J., 2020. Pretreatment of terrestrial macrofossils. Radiocarbon 62 (2), 349–360. https://doi.org/10.1017/RDC.2020.8.
Olsson, I.U., 1983. Dating non-terrestrial materials. In: Proceedings of the First International Symposium 14 C and Archaeology. Groningen, pp. 277–294, 1981 (vol. 8.
Philippsen, B., 2013. The freshwater reservoir effect in radiocarbon dating. Heritage Science 1 (1), 1–19. https://doi.org/10.1186/2050-7445-1-24.
Price, R.C., Gray, C.M., Frey, F.A., 1997. Strontium isotopic and trace element heterogeneity in the plains basalts of the Newer Volcanic Province, Victoria,

Australia. Geochem. Cosmochim. Acta 61 (1), 171–192. https://doi.org/10.1016/S0016-7037(96)00318-3.
Regnéll, J., 1992. Preparing pollen concentrates for AMS dating – a methodological study from a hard-water lake in southern Sweden. Boreas 21 (4), 373–377. https://doi.org/10.1111/j.1502-3885.1992.tb00042.x.
Riding, J.B., 2021. A guide to preparation protocols in palynology. Palynology 45 (S1), 1–110. https://doi.org/10.1080/01916122.2021.1878305.
Rivera-Araya, M., Rowe, C., Levchenko, V., Ulm, S., Bird, M.I., 2022. A radiocarbon chronology for Sanamere Lagoon, Cape York Peninsula, using multiple organic fractions. Quat. Geochronol. 70, 101273. https://doi.org/10.1016/j.quageo.2022.101273.
Rosan, P., Hammarlund, D., 2007. Effects of climate, fire and vegetation development on Holocene changes in total organic carbon concentration in three boreal forest lakes in northern Sweden. Biogeosciences 4 (6), 975–984. https://doi.org/10.5194/bg-4-975-2007.
Rosén, P., Vogel, H., Cunningham, L., Reuss, N., Conley, D.J., Persson, P., 2010. Fourier transform infrared spectroscopy, a new method for rapid determination of total organic and inorganic carbon and biogenic silica concentration in lake sediments. J. Paleolimnol. 43 (2), 247–259. https://doi.org/10.1007/s10933-009-9329-4.
Sanchez-Cabeza, J.A., Ruiz-Fernández, A.C., 2012. 210Pb sediment radiochronology: an integrated formulation and classification of dating models. Geochem. Cosmochim. Acta 82, 183–200. https://doi.org/10.1016/j.gca.2010.12.024.
Schiller, C.M., Whitlock, C., Elder, K.L., Iverson, N.A., Abbott, M.B., 2021. Erroneously old radiocarbon ages from terrestrial pollen concentrates in Yellowstone Lake, Wyoming, USA. Radiocarbon 63 (1), 321–342. https://doi.org/10.1017/RDC.2020.118.
Schneider, L., Pain, C.F., Haberle, S., Blong, R., Alloway, B.V., Fallon, S.J., Hope, G., Zawadzki, A., Heijnis, H., 2019. Evaluating the radiocarbon reservoir effect in Lake Kutubu, Papua New Guinea. Radiocarbon 61 (1), 287–308. https://doi.org/10.1017/RDC.2018.49.
Smith, B.S., Child, D.P., Fierro, D., Harrison, J.J., Heijnis, H., Hotchkis, M.A.C., Johansen, M.P., Marx, S., Payne, T.E., Zawadzki, A., 2016. Measurement of fallout radionuclides , 239 , 240 Pu and creek sediment : Sydney Basin , Australia Cs , in soil and. J. Environ. Radioact. 151, 579–586. https://doi.org/10.1016/j.jenvrad.2015.06.015.
Smith, J.N., 2001. Why should we believe 210Pb sediment geochronologies? J. Environ. Radioact. 55 (2), 121–123. https://doi.org/10.1016/S0265-931X(00)00152-1.
Steinhoff, C., Pickarski, N., Litt, T., Hajdas, I., Welte, C., Wurst, P., Kühne, D., Dolf, A., Germer, M., Kallmeyer, J., 2022. New approach to separate and date small spores and pollen from Lake sediments in semi-arid climates. Radiocarbon 64 (5), 1–17. https://doi.org/10.1017/rdc.2022.34.
Strunk, A., Olsen, J., Sanei, H., Rudra, A., Larsen, N.K., 2020. Improving the reliability of bulk sediment radiocarbon dating. Quat. Sci. Rev. 242, 106442. https://doi.org/10.1016/j.quascirev.2020.106442.
Tennant, R.K., Jones, R.T., Brock, F., Cook, C., Turney, C.S.M., Love, J., Lee, R., 2013. A new flow cytometry method enabling rapid purification of fossil pollen from terrestrial sediments for AMS radiocarbon dating. J. Quat. Sci. 28 (3), 229–236. https://doi.org/10.1002/jqs.2606.
Thakur, P., Khaing, H., Salminen-Paatero, S., 2017. Plutonium in the atmosphere: a global perspective. J. Environ. Radioact. 175–176, 39–51. https://doi.org/10.1016/j.jenvrad.2017.04.008.
Tibby, J., Kershaw, A.P., Builth, H., Philibert, A., White, C., 2006. Environmental change and variability in southwestern Victoria: changing constraints and opportunities for occupation and land use. The social archaeology of Australian indigenous societies 254–269.
Tibby, J., Tyler, J.J., Barr, C., 2018. Post little ice age drying of eastern Australia con fl ates understanding of early settlement impacts 202, 45–52. https://doi.org/10.1016/j.quascirev.2018.10.033.
Timms, B.V., 1976. A comparative study of the limnology of three maar lakes in western Victoria. I. Physiography and physicochemical features. Mar. Freshw. Res. 27 (1), 35–60. https://doi.org/10.1071/MF9760035.
Tims, S.G., Fifield, L.K., Hancock, G.J., Lal, R.R., Hoo, W.T., 2013. Nuclear instruments and methods in physics research B plutonium isotope measurements from across continental Australia. Nuclear Inst. and Methods in Physics Research 294, 636–641. https://doi.org/10.1016/j.nimb.2012.07.010. B.
Tims, S.G., Froehlich, M.B., Fi, L.K., Wallner, A., Cesare, M. De, 2016. U and 239 , 240 Pu ratios from soils around an Australian nuclear weapons test site 151, 563–567. https://doi.org/10.1016/j.jenvrad.2015.06.020.
Toffolo, M.B., 2025. Infrared Spectroscopy of Archaeological Sediments. Cambridge University Press.
Tunno, I., Zimmerman, S.R.H., Brown, T.A., Hassel, C.A., 2021. An improved method for extracting, sorting, and AMS dating of pollen concentrates from Lake sediment. Frontiers in Ecology and Evolution 9 (May). https://doi.org/10.3389/fevo.2021.668676.
Turney, C., Becerra-Valdivia, L., Sookdeo, A., Thomas, Z.A., Palmer, J., Haines, H.A., Cadd, H., Wacker, L., Baker, A., Andersen, M.S., Jacobsen, G., Meredith, K., Chinu, K., Bollhalder, S., Marjo, C., 2021. Radiocarbon protocols and first intercomparison results from the Chronos 14Carbon-Cycle facility. In: University of New South Wales. Radiocarbon, Sydney, Australia, pp. 1003–1023. https://doi.org/10.1017/RDC.2021.23, 63(3).
Tweddle, J.C., Edwards, K.J., 2010. Pollen preservation zones as an interpretative tool in Holocene palynology. Rev. Palaeobot. Palynol. 161 (1–2), 59–76. https://doi.org/10.1016/j.revpalbo.2010.03.004.
Tylmann, W., Bonk, A., Goslar, T., Wulf, S., Grosjean, M., 2016. Calibrating 210Pb dating results with varve chronology and independent chronostratigraphic markers: problems and implications. Quat. Geochronol. 32, 1–10. https://doi.org/10.1016/j.quageo.2015.11.004.
UNSCEAR, 2000. Sources and Effects of Ionizing Radiation: *UNSCEAR 2000 Report to the General Assembly, with Scientific Annexes*, vol. I. United Nations.
Wacker, L., Němec, M., Bourquin, J., 2010. A revolutionary graphitisation system: fully automated, compact and simple. Nuclear Instruments and Methods in Physics Research, Section B: Beam Interactions with Materials and Atoms 268 (7–8), 931–934. https://doi.org/10.1016/j.nimb.2009.10.067.
Wilkins, D., De Deckker, P., Fifield, L.K., Gouramanis, C., Olley, J., 2012. Comparative optical and radiocarbon dating of laminated Holocene sediments in two maar lakes: lake Keilambete and Lake Gnotuk, south-western Victoria, Australia. Quat. Geochronol. 9, 3–15. https://doi.org/10.1016/j.quageo.2012.01.008.
Wolfe, A.P., Miller, G.H., Olsen, C.A., Forman, S.L., Doran, P.T., Holmgren, S.U., 2004. Geochronology of high latitude lake sediments. Long-term Environmental Change in Arctic and Antarctic Lakes. Springer, pp. 19–52. https://doi.org/10.1007/978-1-4020-2126-8_2.
Woodward, C., Shulmeister, J., Bell, D., Haworth, R., Jacobsen, G., Zawadzki, A., 2014. A Holocene record of climate and hydrological changes from Little Llangothlin Lagoon, south eastern Australia. Holocene 24 (12), 1665–1674. https://doi.org/10.1177/0959683614551218.
Wright, H.E., 1967. A square-rod piston sampler for lake sediments. J. Sediment. Res. 37 (3), 975–976. https://doi.org/10.1306/74d71807-2b21-11d7-8648000102c1865d.
Zheng, J., Tagami, K., Watanabe, Y., Uchida, S., Aono, T., Ishii, N., Yoshida, S., Kubota, Y., Fuma, S., Ihara, S., 2012. Isotopic evidence of plutonium release into the environment from the Fukushima DNPP accident. Sci. Rep. 2, 1–8. https://doi.org/10.1038/srep00304.
Zhou, A., He, Y., Wu, D., Zhang, X., Zhang, C., Liu, Z., Yu, J., 2015. Changes in the radiocarbon reservoir age in Lake Xingyun, Southwestern China during the holocene. PLoS One 10 (3), 1–12. https://doi.org/10.1371/journal.pone.0121532.
Zhou, K., Xu, H., Lan, J., Yan, D., Sheng, E., Yu, K., Song, Y., Zhang, J., Fu, P., Xu, S., 2020. Variable late holocene 14C reservoir ages in Lake Bosten, Northwestern China. Front. Earth Sci. 7, 328. https://doi.org/10.3389/feart.2019.00328.
Zimmerman, S.R.H., Brown, T.A., Hassel, C., Heck, J., 2019. Testing pollen sorted by flow cytometry as the basis for high-resolution lacustrine chronologies. Radiocarbon 61 (1), 359–374. https://doi.org/10.1017/RDC.2018.89.
Zimmerman, S.R.H., Wahl, D.B., 2020. Holocene paleoclimate change in the western US: the importance of chronology in discerning patterns and drivers. Quat. Sci. Rev. 246, 106487. https://doi.org/10.1016/j.quascirev.2020.106487.